Article

Cell Chemical Biology

Lenalidomide bypasses CD28 co-stimulation to reinstate PD-1 immunotherapy by activating Notch signaling

Graphical abstract

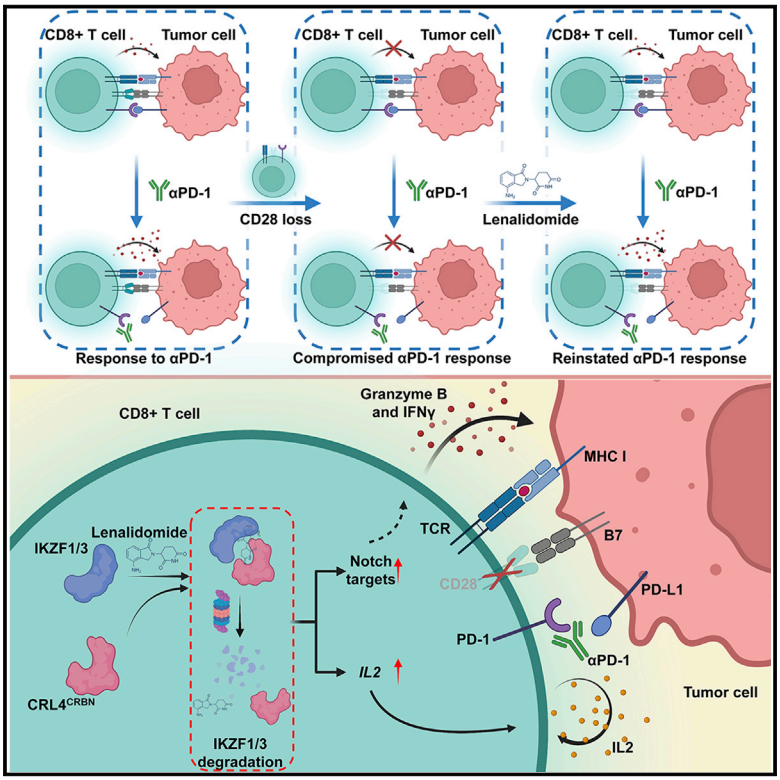

Highlights

- Lenalidomide suppresses tumor growth by activating T cells in *Crbn*^{I391V} mice
- Lenalidomide reinstates PD-1 blockade efficacy compromised by loss of CD28
- Lenalidomide enhances T cell immunity by up-regulating IL-2 and Notch signaling

Authors

Chen-Lu Geng, Jun-Yi Chen, Tian-Yu Song, ..., Qi Zhou, Eui-Cheol Shin, Yong Cang

Correspondence

cangyong@shanghaitech.edu.cn

In brief

Loss of CD28 T cell co-stimulation compromises PD-1 blockade efficacy. Geng et al. use genetically engineered mouse models to demonstrate that lenalidomide, an immunomodulatory drug, reinvigorates CD28-deficient T cells to empower PD-1 immunotherapy against solid tumors.

Geng et al., 2022, Cell Chemical Biology *29*, 1260–1272
August 18, 2022
https://doi.org/10.1016/j.chembiol.2022.05.012

CellPress

CellPress

Cell Chemical Biology

Article

Lenalidomide bypasses CD28 co-stimulation to reinstate PD-1 immunotherapy by activating Notch signaling

Chen-Lu Geng,[1,2,8] Jun-Yi Chen,[2,8] Tian-Yu Song,[2,3] Jae Hyung Jung,[4] Min Long,[1,2] Min-Fang Song,[2] Tong Ji,[5] Byung Soh Min,[6] Jin Gu Lee,[7] Bo Peng,[2] Yi-Sheng Pu,[2] Hong-Jie Fan,[2] Piliang Hao,[2] Qi Zhou,[1] Eui-Cheol Shin,[4] and Yong Cang[2,9,*]

[1]Life Sciences Institute, Zhejiang University, Hangzhou, Zhejiang, China
[2]School of Life Science and Technology, ShanghaiTech University, 393 Middle Huaxia Road, Shanghai 201210, China
[3]Shanghai Institutes for Biological Sciences, Chinese Academy of Sciences, Shanghai, China
[4]Graduate School of Medical Science and Engineering, Korea Advanced Institute of Science and Technology, Daejeon, Republic of Korea
[5]Key Laboratory of Laparoscopic Technique Research of Zhejiang Province, Department of General Surgery, Sir Run Run Shaw Hospital, Zhejiang University School of Medicine, Zhejiang University, Hangzhou, Zhejiang, China
[6]Department of Surgery, Yonsei Cancer Center, Yonsei University College of Medicine, Seoul, Republic of Korea
[7]Department of Thoracic and Cardiovascular Surgery, Severance Hospital, Yonsei University College of Medicine, Seoul, Republic of Korea
[8]These authors contributed equally
[9]Lead contact
*Correspondence: cangyong@shanghaitech.edu.cn
https://doi.org/10.1016/j.chembiol.2022.05.012

SUMMARY

Programmed cell death protein 1 (PD-1) checkpoint blockade therapy requires the CD28 co-stimulatory receptor for $CD8^+$ T cell expansion and cytotoxicity. However, CD28 expression is frequently lost in exhausted T cells and during immune senescence, limiting the clinical benefits of PD-1 immunotherapy in individuals with cancer. Here, using a cereblon knockin mouse model that regains *in vivo* T cell response to lenalidomide, an immunomodulatory imide drug, we show that lenalidomide reinstates the anti-tumor activity of CD28-deficient $CD8^+$ T cells after PD-1 blockade. Lenalidomide redirects the $CRL4^{Crbn}$ ubiquitin ligase to degrade Ikzf1 and Ikzf3 in T cells and unleashes paracrine interleukin-2 (IL-2) and intracellular Notch signaling, which collectively bypass the CD28 requirement for activation of intratumoral $CD8^+$ T cells and inhibition of tumor growth by PD-1 blockade. Our results suggest that PD-1 immunotherapy can benefit from a lenalidomide combination when treating solid tumors infiltrated with abundant $CD28^-$ T cells.

INTRODUCTION

Cytotoxic T lymphocytes recognize tumor antigens and eliminate tumor cells (Boon et al., 1994; Chen and Mellman, 2013; Dunn et al., 2004). Optimal cytotoxic T cell activation requires recognition of the peptide-loaded major histocompatibility complex (MHC) by the T cell receptor (TCR) and a series of co-stimulatory signals (Jenkins et al., 1988). CD28 is an indispensable co-stimulatory receptor required for sufficient T cell activation and effector functions (Esensten et al., 2016). However, CD28-deficient T cells, particularly cytotoxic $CD28^-$ $CD8^+$ T cells, accumulate with age and in solid tumors (Di et al., 2020; Kamphorst et al., 2017; Weng et al., 2009). Almost half of $CD8^+$ T cells are $CD28^-$ in tumors from individuals with non-small cell lung cancer (NSCLC) and colorectal cancer (CRC) (Di et al., 2020; Kamphorst et al., 2017). Loss of CD28 attenuates the T cell response to antigen, and the abundance of $CD28^-$ $CD8^+$ T cells in tumors is associated with advanced disease stage and poor survival (Filaci et al., 2007; Weng et al., 2009). CD28 is dephosphorylated and inactivated in response to PD-1 co-inhibitory receptor signaling (Hui et al., 2017), and CD28 signaling is required for effective programmed cell death protein 1 (PD-1)/PD-L1 immunotherapy in mouse tumor models and individuals with cancer (Kamphorst et al., 2017; Kim et al., 2020). Loss of CD28 on $CD8^+$ T cells compromises T cell-mediated anti-tumor activity and abrogates the clinical benefits of PD-1/PD-L1 blockade. Activating $CD28^-$ $CD8^+$ T cells has the potential to promote the anti-tumor immune response and reinstate the efficacy of PD-1/PD-L1 blockade in solid tumors infiltrated with abundant $CD28^-$ $CD8^+$ T cells.

Lenalidomide is a molecular glue degrader with antineoplastic and immunomodulatory activities. It has been approved to treat multiple myeloma (MM), del(5q) myelodysplastic syndrome (MDS), and several lymphomas in combination with rituximab (Bartlett et al., 2004; Chanan-Khan et al., 2017; Fink et al., 2017; Kronke et al., 2014, 2015; Lu et al., 2014; Witzig et al., 2015). Lenalidomide can kill cancer cells directly by binding to a shallow hydrophobic cavity on cereblon (CRBN) and

redirecting the CRL4^{CRBN} ubiquitin ligase to target essential neosubstrates, including IKZF1, IKZF3, CK1α, and ZFP91 for degradation (An et al., 2017; Kronke et al., 2014, 2015; Lu et al., 2014). Apart from direct cytotoxicity to neoplastic B cells, stimulating T cell and natural killer (NK) cell immunity is another potential mechanism accounting for lenalidomide-mediated anti-tumor activity (Aue et al., 2018; Bartlett et al., 2004; Lagrue et al., 2015). As a single-agent therapy for chronic lymphocytic leukemia (CLL), lenalidomide promotes Th1 cell differentiation and interferon gamma (IFNγ) response (Aue et al., 2018). Lenalidomide and obinutuzumab combination induces an activated T cell phenotype and triggers enrichment for several gene signatures related to effector memory T cell features in individuals with follicular lymphoma (FL) (Menard et al., 2021). Maintenance therapy with lenalidomide activates more myeloma-specific T cell responses and improves NK cell activity in individuals with MM (Besson et al., 2018; Kramer et al., 2016). Enhanced T cell immunity is associated with clinical benefits of lenalidomide in these blood cancers, and it will be attractive to test whether lenalidomide-enhanced T cell immunity can benefit immunotherapy in some solid tumors, especially those infiltrated with abundant CD28$^-$ CD8$^+$ T cells.

Lenalidomide promotes T cell responses in individuals with CLL, FL, and MM (Kramer et al., 2016; Menard et al., 2021) and has the potential to augment multiple T cell-based therapies, such as immune checkpoint blockade, cancer vaccine, and chimeric antigen receptor T (CAR-T) cell therapy (Gorgun et al., 2015; Lapenta et al., 2019; Palma et al., 2018; Wang et al., 2018). However, evaluation of immunomodulatory effects of lenalidomide on these immunotherapies in solid tumors *in vivo* is confounded by the difference in key human and mouse CRBN residues that mediate lenalidomide-induced neo-substrate recruitment (Chamberlain et al., 2014; Kronke et al., 2015). Within the immunomodulatory imide drug (IMiD)-binding domain, the valine at 388 (V388) of human CRBN is critical for lenalidomide-induced degradation of IKZF1, IKZF3, and CK1α (Chamberlain et al., 2014; Kronke et al., 2015). Substitution of the corresponding isoleucine at 391 of mouse Crbn to valine (I391V) re-enables lenalidomide to deplete these substrates and confers lenalidomide-induced cytotoxicity in mouse hematopoietic cells as well as an increase in interleukin-2 (IL-2) in mouse T cells (Fink et al., 2018; Kronke et al., 2015). The *Crbn*^{I391V} mouse model provides us an opportunity to evaluate therapeutic significance of lenalidomide-enhanced T cell response in the context of immunotherapy for solid tumors.

Lenalidomide and its analogs, including thalidomide and pomalidomide, can co-stimulate primary human T lymphocytes, preferentially inducing proliferation, cytokine production, and cytotoxic response in CD8$^+$ T cells in the absence of CD28 co-stimulation signaling *in vitro* (Gandhi et al., 2014; Haslett et al., 1998; LeBlanc et al., 2004). However, it is unknown whether lenalidomide can restore anti-tumor activity and response to PD-1 blockade of intratumoral CD28$^-$ CD8$^+$ T cells. We hypothesized that lenalidomide targets CRBN to activate CD28$^-$ CD8$^+$ T cells, obviating the CD28 requirement for an optimal T cell response and the anti-tumor activity of PD-1/PD-L1 blockers. Here we specifically activate host T cell-mediated anti-tumor immunity by exploiting *Cd28*$^{-/-}$ *Crbn*^{I391V} mice and investigate the co-stimulatory effect of lenalidomide on the host-intrinsic and PD-1 blockade-enhanced T cell response in solid tumors infiltrated with abundant CD28$^-$ CD8$^+$ T cells.

RESULTS

Lenalidomide co-stimulates *Crbn*^{I391V} mouse CD8$^+$ T cells

To recapitulate in mice the co-stimulatory role of lenalidomide in primary human CD8$^+$ T lymphocytes (Haslett et al., 1998), we changed the Ile391 of mouse Crbn to the corresponding Val in human CRBN by CRISPR-Cas9 gene editing in 1- to 2-cell-stage mouse embryos, as described previously (Fink et al., 2018; Gemechu et al., 2018; Kronke et al., 2015). The replacement (Crbn^{I391V}) did not affect the overall survival of newborns or adults (Figure S1A) or interfere with its binding to lenalidomide, as determined by cellular thermal shift assays (CETSAs) (Figures S1B and S1C). The mutation did not alter the development of basic immune cells, such as B cells, myeloid cells, CD4$^+$ T cells, CD8$^+$ T cells, and NK cells (Figures S1D–S1H), or T cell immunity, as indicated by proportions of naive, memory, and effector T cells and regulatory T (Treg) cells (Figures S1I–S1O).

Lenalidomide stimulated dose-dependent activation and proliferation of TCR-ligated CD8$^+$ T cells (Figures 1A and 1B) and, less significantly, CD4$^+$ T cells (Figures S1P and S1Q) isolated from *Crbn*^{I391V} but not wild-type (WT) mouse spleens. Consequently, lenalidomide dramatically increased the cytotoxic response of *Crbn*^{I391V} CD8$^+$ T cells, as indicated by the elevated abundance of secreted IFNγ (Figure 1C) and the increased level of endogenous granzyme B and IFNγ expression (Figure 1D). These T cells, after engineered expression of the OT-1 receptor, killed ovalbumin (OVA)-expressing MC38 mouse CRC cells (Figure 1E) and B16F10 mouse melanoma cells (Figure 1F) more efficiently with lenalidomide treatment in a dose-dependent way. CC-122 and CC-220, two lenalidomide analogs with improved substrate degradation efficacy (Hagner et al., 2015; Matyskiela et al., 2018), stimulated a stronger cytotoxic response and, to a lesser extent, activation than lenalidomide in *Crbn*^{I391V} but not *Crbn*$^{+/+}$ mouse CD8$^+$ T cells (Figures S1R and S1S). Lenalidomide and its analogs promote activation and proliferation of mouse CD8$^+$ T cells by engaging Crbn^{I391V}, leading to enhanced T cell-mediated cytotoxicity against OVA-expressing mouse cancer cells *in vitro*. The Crbn^{I391V} replacement recapitulates in mice the co-stimulatory role of lenalidomide and its analogs in primary human CD8$^+$ T lymphocytes.

Lenalidomide suppresses tumor growth by targeting CD8$^+$ T cells

To determine the anti-tumor activity of lenalidomide-activated T cells *in vivo*, C57BL/6 mouse-derived MC38-OVA cells were implanted into WT and *Crbn*^{I391V} C57BL/6 mice, followed by treatment with lenalidomide or vehicle (CMC) control. Lenalidomide suppressed growth of tumors implanted in *Crbn*^{I391V} mice only, and suppression was abrogated after depletion of host T cells induced by anti-CD4 and anti-CD8 antibodies (Figure 2A). Flow cytometry analysis of the tumor-infiltrating lymphocytes (TILs) revealed that lenalidomide treatment increased the population of highly cytotoxic (granzyme B^{high}) CD8$^+$ T cells in tumors specifically from *Crbn*^{I391V} mice (Figure 2B). Depletion of CD8$^+$ but not CD4$^+$ T cells abolished lenalidomide-induced

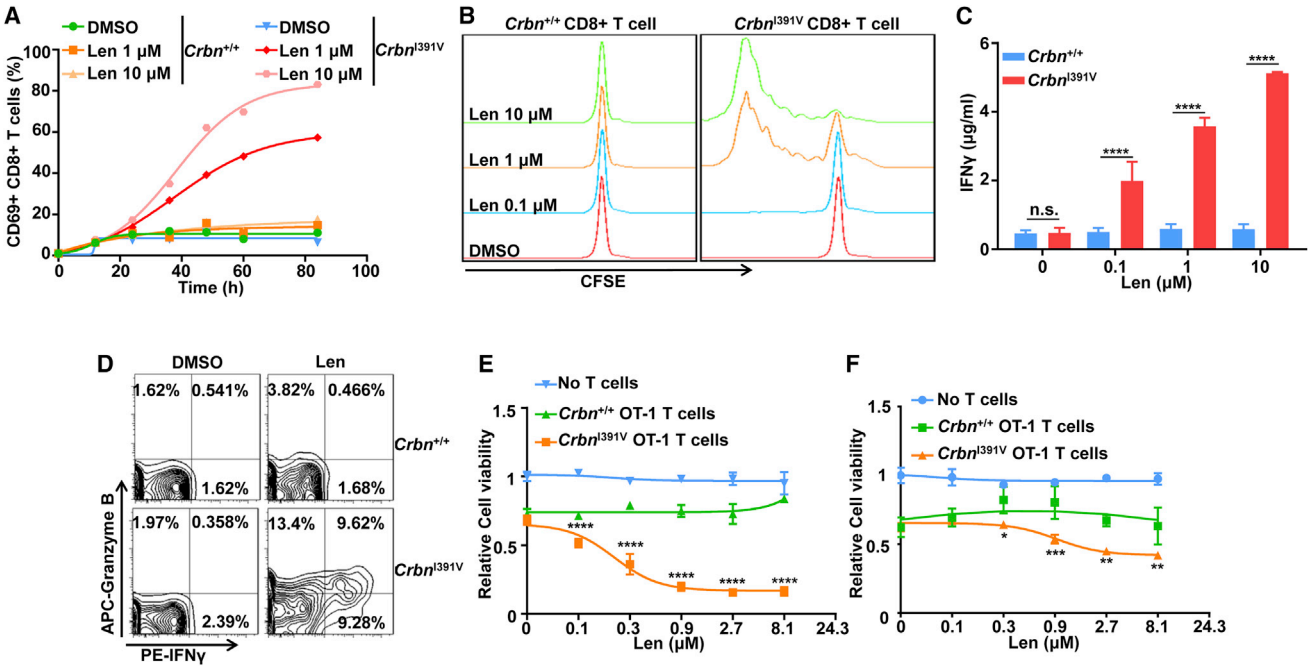

Figure 1. Lenalidomide promotes activation and cytotoxicity of CD8$^+$ T cells from *Crbn*^{I391V} mice

(A) Percentage of CD69$^+$ cells among CD8$^+$ T cells after *ex vivo* stimulation with immobilized αCD3e antibody in the presence of lenalidomide (Len) or vehicle control (DMSO) for 24 h.

(B) Cell proliferation measured by CFSE (carboxy fluorescein diacetate, succinimidyl ester, fluorescent probe reagent) dilution of CD8$^+$ T cells after *ex vivo* stimulation with immobilized αCD3e antibody in the presence of Len or vehicle control (DMSO) for 96 h.

(C) IFNγ release of CD8$^+$ T cells after *ex vivo* stimulation with immobilized αCD3e antibody in the presence of increasing doses of Len for 96 h.

(D) Cytotoxic response indicated by IFNγ and granzyme B staining of CD8$^+$ T cells after *ex vivo* stimulation with immobilized αCD3e antibody in the presence of 1 μM Len or vehicle control (DMSO) for 96 h.

(E and F) Relative cell viability of MC38-OVA (E) and B16F10-OVA (F) cancer cells that were co-cultured with OT-1 CD8$^+$ T cells in the presence of increasing doses of Len for 72 h (n = 3).

Data are mean ± SD (C, E, and F). n indicates biological replicates (C, E, and F). All experiments were performed at least three times, and representative data of one experiment are shown. The p values were determined by multiple t tests (C, E, and F). n.s., no significance. *p < 0.05, **p < 0.01, ***p < 0.001, ****p < 0.0001.

tumor regression in *Crbn*^{I391V} mice (Figures 2C and S2A–S2D). The abundance of total immune cells, CD8$^+$ T cells, or CD4$^+$ T cells, including T helper 1 (Th1) cells and Treg cells, did not change in response to lenalidomide treatment in tumors from both host strains (Figures S2E–S2I). In contrast, lenalidomide promoted activation and proliferation of peripheral CD8$^+$ and CD4$^+$ T cells from *Crbn*^{I391V} mouse spleens (Figures 2D, 2E, S2J, and S2K). Differentiation of Th1 and Treg cells was increased after lenalidomide treatment in *Crbn*^{I391V} mouse spleens (Figures S2L and S2M). These data indicate that lenalidomide activates the T cell response systemically in *Crbn*^{I391V} mice. Because the compound did not inhibit MC38-OVA cell proliferation (Figure 1E) or tumor growth in the WT host (Figure 2A), we conclude that lenalidomide exerts its anti-tumor activity by engaging Crbn^{I391V} and activating cytotoxic CD8$^+$ T cells.

To extend the general applicability of lenalidomide-enhanced T cell antitumor immunity, we treated B16F10-OVA mouse melanoma established in *Crbn*^{I391V} mice with lenalidomide, anti-mouse PD-1 antibody (αPD-1), or both. Unlike single-agent treatment, combination treatment with lenalidomide and αPD-1 suppressed tumor growth (Figures S3A–S3C). Mechanistically, lenalidomide combined with αPD-1 enhanced infiltration of total immune cells and cytotoxicity of tumor-infiltrating CD8$^+$ T cells in B16F10-OVA tumors (Figures S3D and S3E), without affecting the number of CD4$^+$, CD8$^+$ T cells or the abundance and cytotoxicity of terminally exhausted (PD-1+ TIM3+) CD8$^+$ T cells (Figures S3F–S3I). Lenalidomide promoted activation of peripheral CD4$^+$ T cells but not CD8$^+$ T cells from tumor-bearing mouse spleens (Figures S3J and S3K). In another syngeneic model, 3LL mouse lung cancer, lenalidomide failed to suppress tumor growth, promote activation of peripheral CD8$^+$ T cells, or affect tumor infiltration of total immune cells, myeloid cells, and T cells (Figures S3L–S3P). Although lenalidomide cannot suppress growth of B16F10-OVA or 3LL tumors, it can sensitize B16F10-OVA tumors to PD-1 blockade in *Crbn*^{I391V} mice.

Lenalidomide co-stimulates CD28-deficient CD8$^+$ T cells

Next we sought to determine whether lenalidomide can co-stimulate T cells independent of the CD28 co-stimulatory receptor in the *Crbn*^{I391V} mouse model. Upon TCR and CD28 ligation, lenalidomide elevated *Crbn*^{I391V} CD8$^+$ T cell activation and cytotoxic response (Figures 3A and 3B). With the co-stimulatory signal delivered by a soluble anti-CD28 antibody, lenalidomide still enhanced OT-1 *Crbn*^{I391V} CD8$^+$ T cell cytotoxicity against MC38-OVA and B16F10-OVA cancer cells (Figures 3C and 3D).

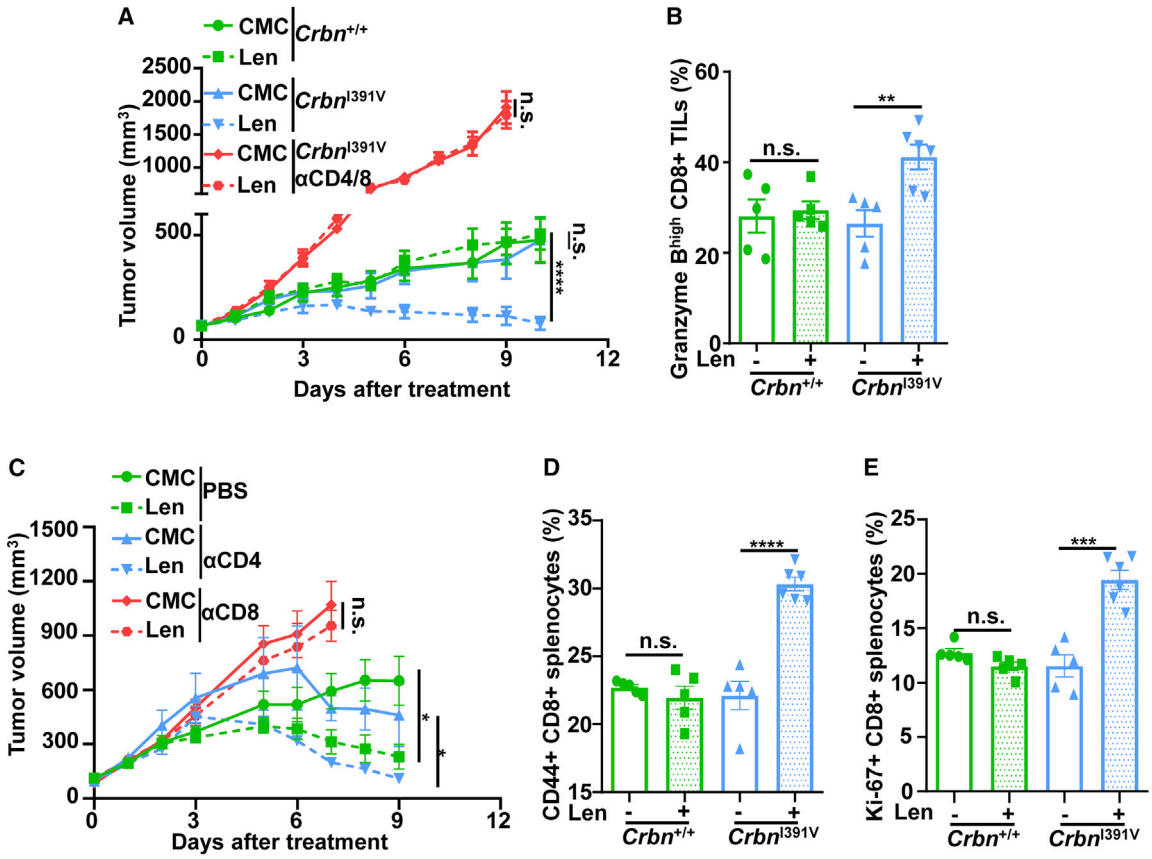

Figure 2. Len suppresses tumor growth in *Crbn*^{I391V} mice by targeting CD8$^+$ T cells

(A) Caliper-determined tumor volumes of MC38-OVA tumors grown subcutaneously in mice, treated with 50 mpk (milligram per kilogram) Len or vehicle control (CMC), with at least four mice per group.

(B) Quantification of the highly cytotoxic (granzyme B^{high}) CD8$^+$ T cell population in tumors from tumor-bearing mice in (A), which were assessed by flow cytometric analysis with at least four mice per group.

(C) Caliper-determined tumor volumes of MC38-OVA tumors grown subcutaneously in *Crbn*^{I391V} mice, treated with 50 mpk Len or vehicle control (CMC), with at least four mice per group.

(D and E) Quantification of splenocytes from tumor-bearing mice in (A). Cell populations were identified as activated (CD44$^+$) (G) and proliferative (Ki-67$^+$) (H) CD8$^+$ T cells, with at least five mice per group.

Data are mean ± SEM All experiments were performed at least three times, and representative data of one experiment are shown. The p values were determined by unpaired t tests. *p < 0.05, **p < 0.01, ***p < 0.001, ****p < 0.0001.

Lenalidomide-induced *Crbn*^{I391V} CD8$^+$ T cell activation was compensated, but not completely, by saturating levels of CD28 co-stimulation (Figures 3E and S4A). Differential gene expression after lenalidomide treatment is highly correlated with that induced by CD28 co-stimulation in *Crbn*^{I391V} but not WT CD8$^+$ T cells (Figures 3F and 3G), up-regulating MYC and E2F signaling, the G2/M cell cycle checkpoint, IL-2-STAT5 signaling, and mechanistic target of rapamycin (mTOR) response (Figures S4B and S4C). Compared with CD28 ligation, the compound treatment also up-regulated type 1 and 2 IFN and the tumor necrosis factor alpha (TNF-α)-nuclear factor κB (NF-κB) pathways (Figures S4B and S4C), as reflected by more differentially expressed genes, including *Ccl1*, *Ccl9*, *Ifitm3*, and *Ccl22* (Figure 3G). These results suggest that lenalidomide co-stimulates CD8$^+$ T cells at least in part independent of the CD28 receptor and mimics CD28 ligation-induced transcription changes in CD8$^+$ T cells.

Next we sought to determine whether lenalidomide can co-stimulate CD28-deficient CD8$^+$ T cells. Interestingly, genetic deletion of CD28 in *Crbn*^{I391V} CD4$^+$ and CD8$^+$ T cells (Figure S4D) slightly attenuated T cell activation in response to the anti-CD3e antibody but had no effect on lenalidomide-promoted activation (Figures 3H and S4E). Then we tested the co-stimulatory effect of lenalidomide in CD8$^+$ T cells isolated from samples from individuals with CRC. In aged individuals with CRC, CD28 deficiency accounted for more than half of the CD8$^+$ T cells in peripheral blood mononuclear cells (PBMCs) (52% ± 10%; n = 9; age, 61 ± 13 years) and even more in TILs (60% ± 18%; n = 7; age, 61 ± 10 years) (Figures S4F and S4G). Lenalidomide increased the percentage of activated T cells in CD28$^-$ and CD28$^+$ CD8$^+$ T cell populations isolated from these PBMCs (Figure 3I). These results suggest that lenalidomide can co-stimulate CD28-deficient CD8$^+$ T cells *in vitro*.

Lenalidomide restores anti-tumor immune response compromised by CD28 deficiency

Next we sought to determine whether lenalidomide can reinvigorate the anti-tumor activity of CD28$^-$ CD8$^+$ T cells in tumors. First

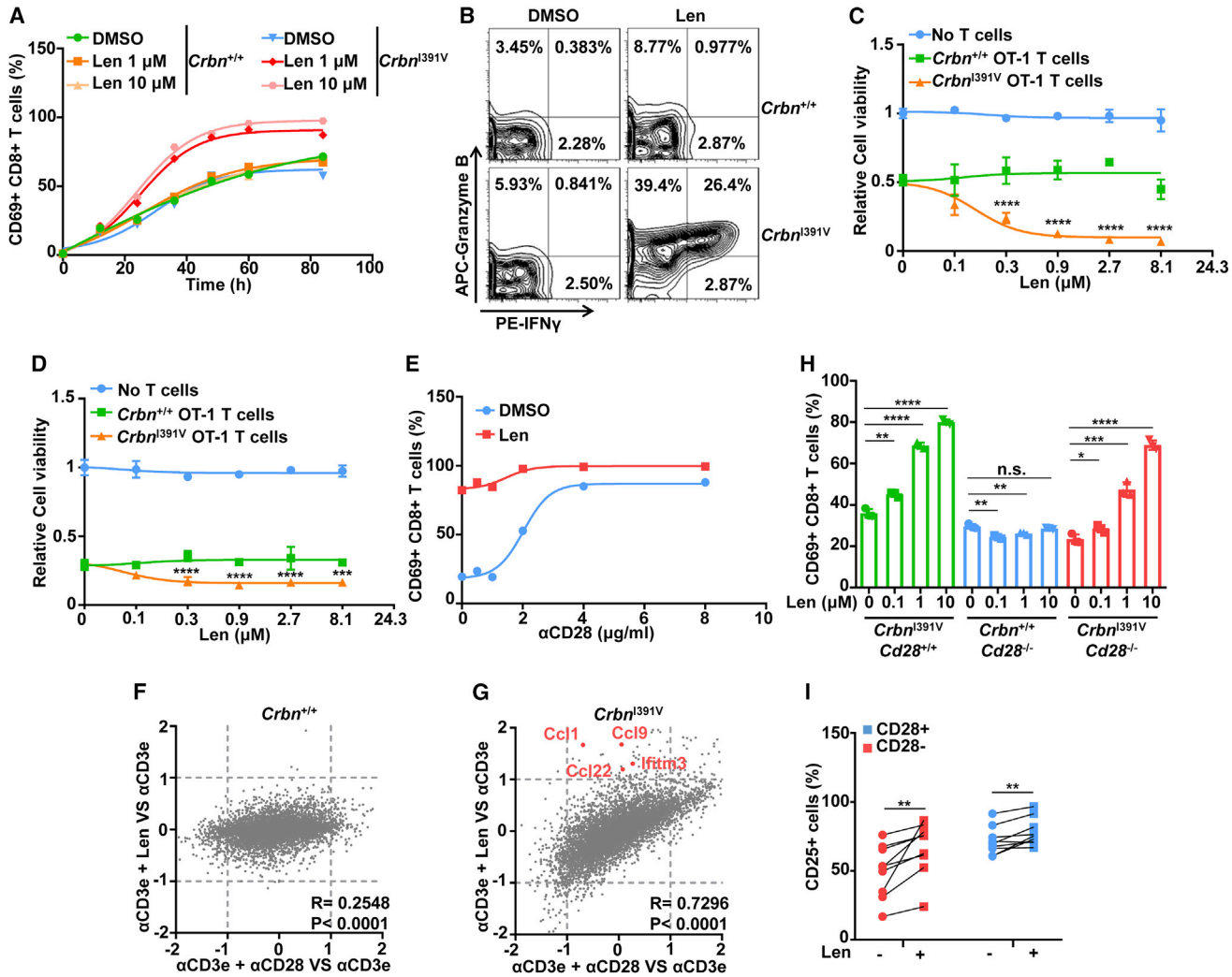

Figure 3. Len stimulates CD28-independent T cell activation

(A) Percentage of CD69$^+$ cells among CD8$^+$ T cells after *ex vivo* stimulation with immobilized αCD3e and soluble αCD28 antibodies in the presence of Len or vehicle control (DMSO) for 24 h.

(B) Percentage of IFNγ^{high} granzyme B^{high} cells among CD8$^+$ T cells after *ex vivo* stimulation with immobilized αCD3e and soluble αCD28 antibodies in the presence of 1 μM Len or vehicle control (DMSO) for 96 h.

(C and D) Relative cell viability of MC38-OVA (C) and B16F10-OVA (D) cancer cells that were co-cultured with OT-1 CD8$^+$ T cells in the presence of 2 μg/mL soluble αCD28 antibody and increasing doses of Len for 72 h (n = 3).

(E) Percentage of CD69$^+$ cells among *Crbn*^{I391V} CD8$^+$ T cells after *ex vivo* stimulation with immobilized αCD3e and increasing doses of soluble αCD28 antibodies in the presence of 5 μM Len or vehicle control (DMSO) for 24 h.

(F and G) Correlation of gene expression profiles of 5 μM Len and 4 μg/mL αCD28 co-stimulated CD8$^+$ T cells from *Crbn*$^{+/+}$ (F) or *Crbn*^{I391V} (G) mice. Data are plotted using Log_2 fold change (Log_2FC).

(H) Percentage of CD69$^+$ cells among CD8$^+$ T cells after *ex vivo* stimulation with immobilized αCD3e antibody in the presence of increasing doses of Len for 48 h (n = 3).

(I) Percentage of activated (CD25$^+$) cells among peripheral CD8$^+$ T cells from individuals with CRC after stimulation with 1 ng/mL soluble αCD3 antibody in the presence of 5 μM Len or left unstimulated for 108 h (n = 9).

Data are mean ± SD (C, D, and H). n indicates biological replicates (C, D, and H) or number of individuals with CRC (I). For (A)–(E), (H), and (I), experiments were performed at least three times, and representative data of one experiment are shown. The p values were determined by multiple t tests (C, D, and H) or paired t test (I). *p < 0.05, **p < 0.01, ***p < 0.001, ****p < 0.0001.

we found that MC38 tumors grew faster in CD28-deficient mice but responded to lenalidomide inhibition even better than WT mice when harboring *Crbn*^{I391V} (Figure 4A). Knockout of CD28 decreased infiltration of total immune cells, CD8$^+$ T cells, and CD4$^+$ T cells in tumors (Figures 4B, 4C, and S5A). TIL analysis found increased infiltration of total immune cells and CD8$^+$ T cells, particularly those expressing high granzyme B, but no effect on CD4$^+$ T cells in tumors from CD28-deficient *Crbn*^{I391V} mice treated with lenalidomide (Figures 4B–4D and S5A). The systemic effects of the compound in these tumor-bearing mouse

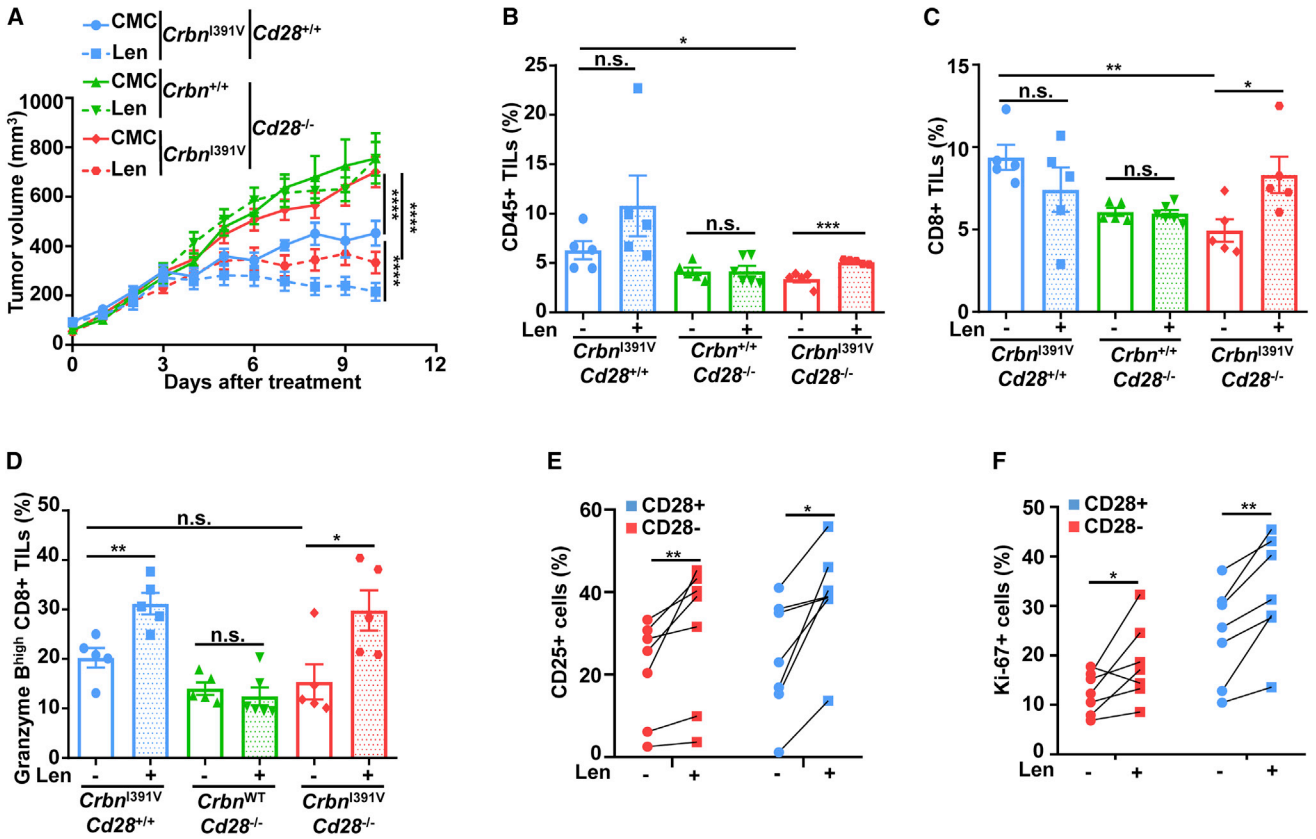

Figure 4. Len restores anti-tumor immunity compromised by CD28 loss

(A) Caliper-determined tumor volumes of MC38-OVA tumors grown subcutaneously in mice, treated with 50 mpk Len or vehicle control (CMC), with at least five mice per group.

(B–D) Quantification of TILs from tumor-bearing mice in (A), which were assessed by flow cytometry analysis. Cell populations were identified as total immune ($CD45^+$) cells (B), $CD8^+$ T cells (C), and cytotoxic ($CD8^+$ granzyme B^{high}) T cells (D), with at least five mice per group.

(E and F) Percentage of activated ($CD25^+$) (E, n = 7) and proliferative ($Ki\text{-}67^+$) (F, n = 7) cells in tumor-infiltrating $CD8^+$ T cells from individuals with CRC after stimulation with 1 ng/mL soluble αCD3 antibody in the presence of 5 μM Len treatment or no treatment.

Data are mean ± SEM (A–D). All experiments were performed at least three times, and representative data of one experiment are shown. The p values were determined by unpaired t tests (A–D) or paired t tests (E and F). *p < 0.05, **p < 0.01, ***p < 0.001, ****p < 0.0001.

spleens were more dramatic, as evidenced by partial rescue of the defective activation and proliferation of $CD4^+$ and $CD8^+$ T cells and poor differentiation of Th1 and Treg cells in the absence of CD28 (Figures S5B–S5G). Second, we evaluated the effect of lenalidomide on $CD28^-$ and $CD28^+$ $CD8^+$ T cells isolated from tumors of individuals with CRC. Lenalidomide increased the percentage of activated and proliferating T cells in $CD28^-$ and $CD28^+$ $CD8^+$ T cell populations isolated from these TILs (Figures 4E and 4F). These results indicate that lenalidomide restores the anti-tumor activity of $CD28^-$ $CD8^+$ T cells and suppresses overgrowth of tumors induced by loss of CD28 in the mouse model.

Lenalidomide reinstates response to PD-1 blockade of $CD28^-$ $CD8^+$ T cells

To determine whether lenalidomide can restore PD-1 blockade efficacy in *Cd28*$^{-/-}$ *Crbn*^{I391V} mice, we performed lenalidomide and αPD-1 combination treatment in the established MC38-OVA model. We reaffirmed that loss of CD28 abolished the anti-tumor activity of PD-1 blockade (Hui et al., 2017; Kamphorst et al., 2017) but found that lenalidomide completely reinstated PD-1 immunotherapy compromised by CD28 deficiency (Figures 5A and S5H–S5K). Blocking PD-1 increased lenalidomide-induced infiltration of highly cytotoxic $CD8^+$ T cells (Figure 5B) with no change in total TIL, $CD8^+$ T cell, or terminally exhausted $CD8^+$ T cell numbers (Figures 5C, 5D, and S5L). All of these results suggest that lenalidomide treatment can restore PD-1 blockade efficacy compromised by loss of CD28.

We also performed lenalidomide and αPD-1 combination treatment in $CD8^+$ T cells isolated from tumors of individuals with CRC. Lenalidomide increased the percentage of activated ($CD25^+$) T cells in $CD28^-$and $CD28^+$ $CD8^+$ T cells, which was not increased further by combination αPD-1 treatment (Figure 5E). In assays for proliferating ($Ki\text{-}67^+$) T cells, lenalidomide also increased the proliferative response of all $CD8^+$ T cells (Figure 5F). Lenalidomide and αPD-1 combination treatment further increased the proliferative response of $CD28^-$ but not $CD28^+$ $CD8^+$ T cells compared with lenalidomide single-agent treatment (Figure 5F), justifying future clinical studies to examine

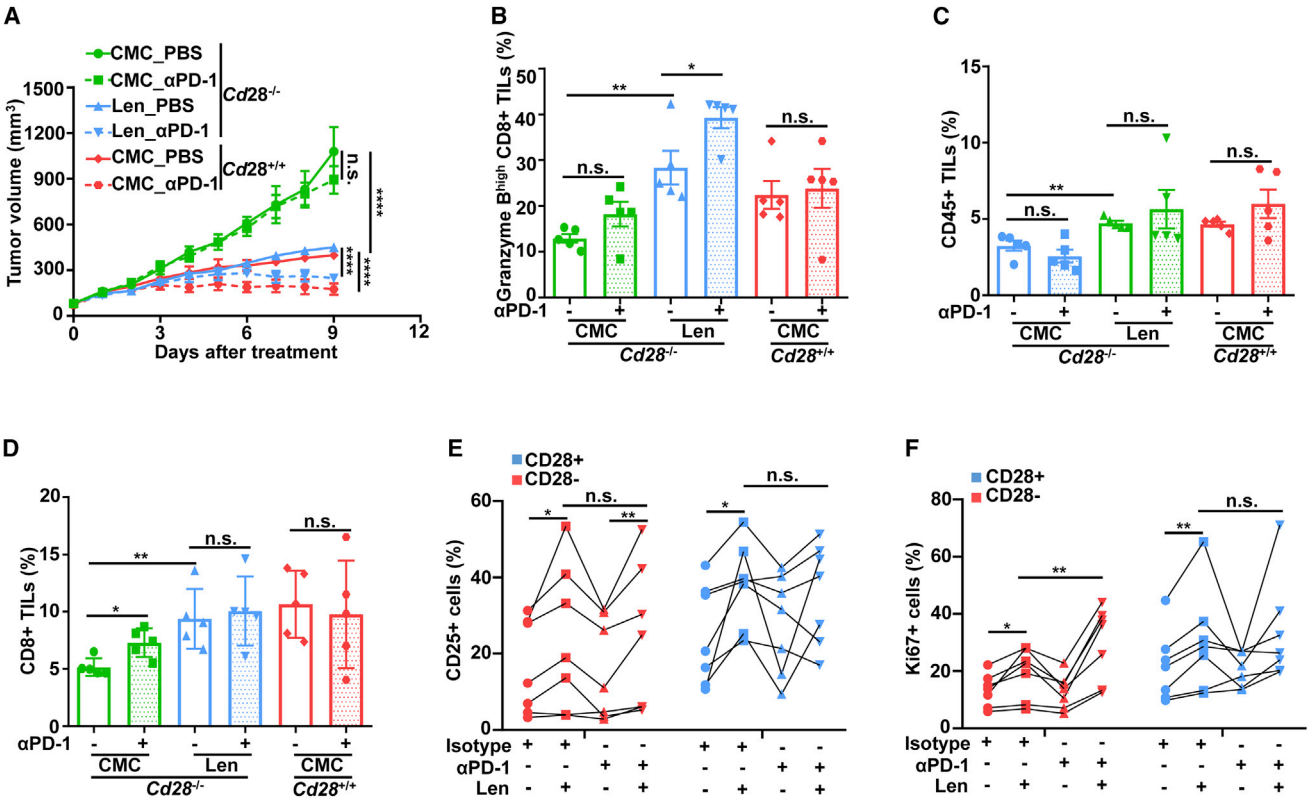

Figure 5. Len reinstates PD-1 blockade efficacy compromised by CD28 loss

(A) Caliper-determined tumor volumes of MC38-OVA tumors grown subcutaneously in *Crbn*^{I391V} mice, treated with Len (Len_PBS), αPD-1 (CMC_αPD-1), combination (Len_αPD-1), or vehicle control (CMC_PBS), with at least five mice per group.

(B–D) Quantification of TILs from tumor-bearing mice in (A), which were assessed by flow cytometry analysis. Cell populations were identified as cytotoxic (CD8$^+$ granzyme B^{high}) T cells (B), total immune (CD45$^+$) cells (C), and CD8$^+$ T cells (D), with five mice per group.

(E and F) Percentage of activated (CD25$^+$) (E, n = 7) and proliferative (Ki-67$^+$) (F, n = 7) cells in tumor-infiltrating CD8$^+$ T cells after stimulation with irradiated non-CD8$^+$ cells from tumors from individuals with CRC in the presence of 5 μM Len and 10 μg/mL aPD-1 antibody treatment for 108 h.

Data are mean ± SEM (A–D). All experiments were performed at least three times, and representative data of one experiment are shown. The p values were determined by unpaired t tests (A–D) or paired t tests (E and F). *p < 0.05, **p < 0.01, ****p < 0.0001.

combining lenalidomide with PD-1 blockers to treat CRC infiltrated with abundant CD28$^-$ CD8$^+$ T cells.

Lenalidomide co-stimulates CD8$^+$ T cells in part by up-regulating IL-2

To unravel the CD28 downstream effectors activated by lenalidomide, we interrogated the proteomics and transcriptomics of *Crbn*^{I391V} T cells upon lenalidomide treatment *in vitro*. Blocking cullin-mediated ubiquitination activity with MLN4924 abrogated lenalidomide-induced but not CD28-stimulated T cell activation (Figure 6A). Correspondingly, non-labeled whole-cell proteomics analysis identified Ikzf1 and Ikzf3 robustly depleted specifically in *Crbn*^{I391V} T cells treated with lenalidomide or pomalidomide and Ck1α with lenalidomide only (Figure 6B), consistent with previous IMiD studies in human cells (Kronke et al., 2014, 2015; Lu et al., 2014). Lenalidomide and pomalidomide induced similar transcriptomic changes and enriched the same sets of genes that up-regulate inflammatory and IFN responses, IL-2 and TNF-α signaling, and MYC/E2F targets in *Crbn*^{I391V} T cells (Figures 6C, 6D, and S6A). Compared with lenalidomide and pomalidomide, thalidomide is much less effective in Crbn^{I391V}-dependent degradation of Ikzf1 and Ikzf3 or stimulation of CD8$^+$ and CD4$^+$ T cell proliferation *in vitro* (Figures 6E, S6B, and S6C). Ikzf3 levels were also reduced in T cells from splenocytes and TILs of lenalidomide-treated *Crbn*^{I391V} mice (Figures S6D–S6F). All of these results suggest that lenalidomide and pomalidomide co-stimulate T cells by inducing degradation of IKZF1 and IKZF3, consistent with a previous study in primary human T cells (Gandhi et al., 2014).

IKZF1 and IKZF3 repress IL-2 transcription (Bandyopadhyay et al., 2007; Quintana et al., 2012), and their knockdown mimics IMiD-induced IL-2 elevation in human T cells (Gandhi et al., 2014). We found that lenalidomide induced a dose-dependent increase of secreted IL-2 by targeting Crbn^{I391V} (Figure 6F), and blocking IL-2 signaling with a neutralizing antibody decreased but failed to completely block lenalidomide-induced activation of *Crbn*^{I391V} CD8$^+$ T cells (Figure 6G). To evaluate the paracrine effect of lenalidomide-induced IL-2 secretion, we mixed WT and *Crbn*^{I391V} mouse CD8$^+$ T cells for an activation assay (Figure S6G). Treating co-cultured CD45.1 WT and CD45.2 *Crbn*^{I391V} CD8$^+$ T cells with

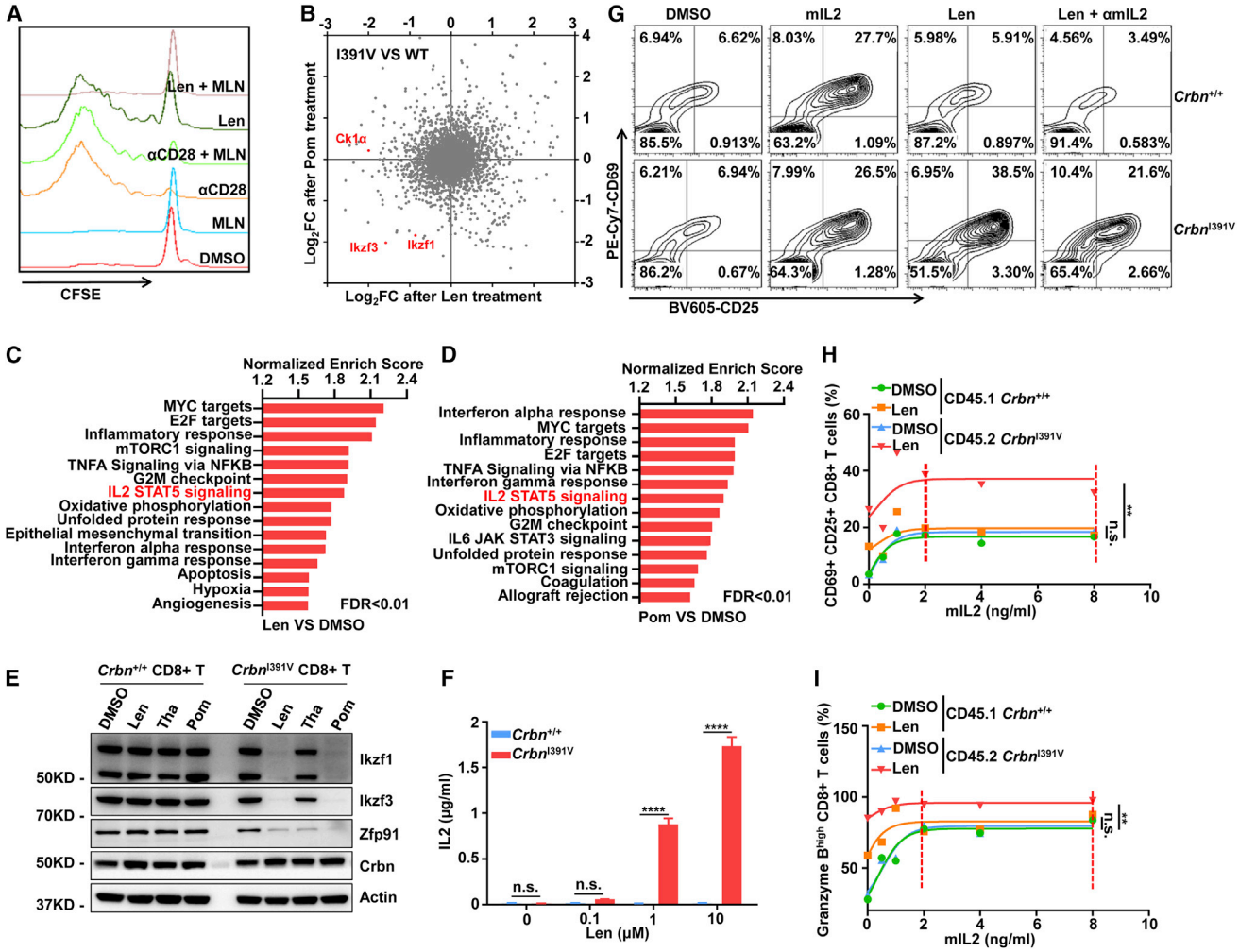

Figure 6. Len co-stimulates CD8$^+$ T cells in part by up-regulating IL-2 secretion

(A) Cell proliferation of *Crbn*^{I391V} CD8$^+$ T cells measured by CFSE dilution after *ex vivo* stimulation with immobilized αCD3e antibody in the presence of 5 μM Len, 400 nM MLN4924 (MLN), and 2 μg/mL soluble αCD28 antibody for 96 h.

(B) Changes of protein abundance, determined by liquid chromatography-mass spectrometry in CD8$^+$ T cells after *ex vivo* stimulation with immobilized αCD3e antibody in the presence of 10 μM Len and 1 μM pomalidomide (Pom) for 24 h.

(C and D) Gene set enrichment analysis (GSEA) of RNA-sequencing (RNA-seq) data of *Crbn*^{I391V} CD8$^+$ T cells after *ex vivo* stimulation with immobilized αCD3e antibody for 24 h in the presence of 10 μM Len (C) or 1 μM Pom (D).

(E) Immunoblot analysis of CD8$^+$ T cells after treatment with 10 μM Len, 50 μM thalidomide (Tha), or 1 μM Pom for 24 h.

(F) IL-2 release in the supernatant of CD8$^+$ T cells after *ex vivo* stimulation with immobilized αCD3e antibody in the presence of increasing doses of Len for 96 h (n = 3).

(G) Percentage of CD25$^+$ CD69$^+$ cells among CD8$^+$ T cells after *ex vivo* stimulation with immobilized αCD3e antibody for 24 h in the presence of 2 ng/mL mouse IL-2 (mIL2), 1 μM Len, or 2 μg/mL αIL-2 antibody.

(H) Percentage of CD25$^+$ CD69$^+$ cells among mixed CD8$^+$ T cells after stimulation with immobilized αCD3e antibody in the presence of 1 μM Len and increasing doses of mIL-2 for 24 h.

(I) Percentage of granzyme B^{high} cells among mixed CD8$^+$ cells after stimulation with immobilized αCD3e antibody in the presence of 1 μM Len and increasing doses of mIL-2 for 96 h.

Data are mean ± SD (F). n indicates biological replicates (F). For (A) and (E)–(I), experiments were performed at least three times, and representative data of one experiment are shown. The p values were determined by unpaired t tests (F, H, and I), and the data of saturated IL-2 treatment were used for analysis (H and I). **p < 0.01, ****p < 0.0001.

lenalidomide enhanced paracrine activation and the cytotoxic response of WT T cells, which can be offset by saturating recombinant IL-2 and blocked by an IL-2-neutralizing antibody (Figures 6H, 6I, and S6H–S6M). Exogenous IL-2 could never stimulate WT T cells to reach the activation and cytotoxicity levels of lenalidomide-treated *Crbn*^{I391V} T cells, even with CD28 co-stimulation (Figures 6H, 6I, S6H, and S6I). These results suggest that lenalidomide targets CRBN to activate IL-2-dependent and IL-2-independent signaling for CD28-independent T cell activation.

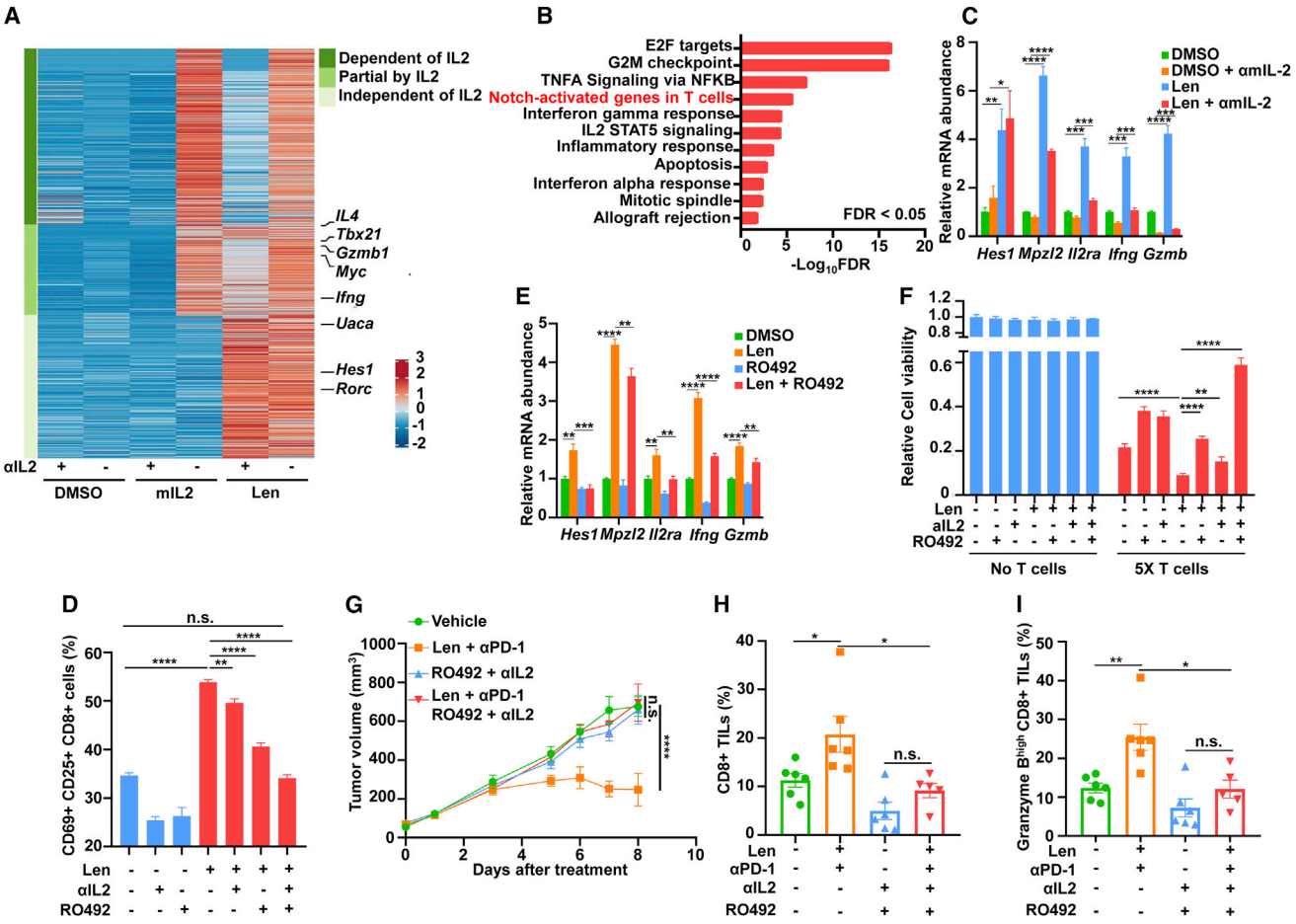

Figure 7. Len and αPD-1 antibody combination therapy requires IL-2 and Notch signaling

(A) Transcriptome analysis of *Crbn*^{I391V} CD8$^+$ T cells after *ex vivo* stimulation with immobilized αCD3e antibody in the presence of 2 ng/mL mIL-2, 10 μM Len, or 2 μg/mL αIL-2 antibody for 24 h. The cluster represents probe sets whose expression increased more than 1.6-fold after Len treatment. The color scale represents standardized fold changes.

(B) Pathway analysis of 1,287 differentially expressed Len-induced but IL-2-independent genes in *Crbn*^{I391V} CD8$^+$ T cells.

(C) Validation of RNA-seq data by qRT-PCR analysis (n = 3).

(D) Percentage of CD25$^+$ CD69$^+$ cells in *Crbn*^{I391V} CD8$^+$ T cells after *ex vivo* stimulation with immobilized αCD3e antibody in the presence of 5 μM Len, 2 μg/mL αIL-2 antibody, and 1 μM RO4929097 (RO492) for 24 h (n = 3).

(E) qRT-PCR analysis of some known Notch-activated genes in *Crbn*^{I391V} CD8$^+$ T cells after stimulation with immobilized αCD3e antibody in the presence of 5 μM Len and 1 μM RO492 for 24 h (n = 3).

(F) Relative cell viability of MC38-OVA cancer cells that were co-cultured with *Crbn*^{I391V} OT-1 T cells in the presence of 5 μM Len, 2 μg/mL αIL-2 antibody, and 1 μM RO492 for 72 h (n = 3).

(G) Caliper-determined tumor volumes of MC38-OVA tumors grown subcutaneously in *Cd28*$^{-/-}$ *Crbn*^{I391V} mice with treatment of Len combined with αPD-1 (Len + αPD-1), αIL-2 plus Notch inhibitor (αIL2 + RO492), or vehicle control, with at least five mice per group.

(H and I) Quantification of TILs from tumor-bearing mice in (G), which were assessed by flow cytometry analysis. Cell populations were identified as CD8$^+$ T cells (H) and cytotoxic (CD8$^+$ granzyme B^{high}) T cells (I), with at least five mice per group.

Data are mean ± SD (C–F) or SEM (G–I). n indicates biological replicates (C–F). For (C)–(I), experiments were performed at least three times, and representative data of one experiment are shown. The p values were determined by unpaired t tests (D and F–I). *p < 0.05, **p < 0.01, ****p < 0.0001.

Lenalidomide and PD-1 blockade combination therapy requires IL-2 and Notch signaling

To identify these IL-2-independent effectors, we analyzed the transcriptomics of *Crbn*^{I391V} CD8$^+$ T cells stimulated with IL-2 or lenalidomide in the presence or absence of an IL-2-blocking antibody (Figures S7A and S7B). Among 1,287 up-regulated lenalidomide-induced but IL-2-independent genes (Figure 7A), significant enrichment of IKZF1-suppressed Notch targets in T cells (Geimer Le Lay et al., 2014) was identified (Figures 7B and S7C). Expression of selected Notch-activated genes, including *Hes1*, *Mpzl2*, and *Tbx21*, was validated independently (Figure 7C). We inactivated *IKZF1* or *IKZF3* in Jurkat human T cells by CRISPR-Cas9 (Figure S7D) and demonstrated that loss of either protein up-regulated expression of *IL2* and Notch-activated genes such as *HES1*, *MPZL2*, and *IL2RA*, as observed with lenalidomide treatment (Figures S7E–S7H). Therefore, we conclude that lenalidomide induces degradation of IKZF1 and IKZF3 to release suppression of Notch-activated genes in T cells.

Finally, we investigated the role of IL-2 and Notch activation in the lenalidomide-enhanced T cell response. A chemical inhibitor of Notch signaling (RO4929097; Paolini et al., 2021) attenuated activation and the cytotoxic response of *Crbn*^{I391V} CD8$^+$ T cells treated with lenalidomide and almost completely abolished these T cell activities when combined with an IL-2-blocking antibody (Figures 7D and S7I). Another Notch inhibitor (IMR-1; Cheng et al., 2021) with a distinct mechanism similarly dampened lenalidomide-enhanced T cell activation (Figures S7J and S7K). Lenalidomide-stimulated expression of Notch target genes was decreased upon Notch inhibition (Figure 7E). As a result, lenalidomide-enhanced killing of MC38-OVA cancer cells by *Crbn*^{I391V} OT-1 CD8$^+$ T cells was suppressed by the Notch inhibitor or IL-2 antibody and more prominently by their combination (Figure 7F). Conversely, activating Notch in CD8$^+$ T cells with recombinant mouse Delta-like 1 (rmDll1; Kakuda et al., 2020) stimulated T cell activation in the absence of CD28 co-stimulation (Figures S7L and S7M).

Strikingly, lenalidomide-reinstated anti-tumor activity of PD-1 blockade in CD28-deficient *Crbn*^{I391V} mice was completely abrogated by blocking Notch and IL-2 signaling (Figures 7G and S7N). TIL analysis confirmed that dual Notch and IL2 inhibition counteracted the lenalidomide-induced increase in the number and cytotoxicity of CD8$^+$ T cells as well as total TILs in *Cd28*$^{-/-}$ *Crbn*^{I391V} mice (Figures 7H, 7I, and S7O), with no effect on the levels of lenalidomide-targeted substrates (Figures S7P and S7Q). The systemic effects of lenalidomide in these tumor-bearing mouse spleens were also abrogated by dual Notch and IL-2 inhibition, as indicated by decreased numbers of activated CD4$^+$ and CD8$^+$ T cells and poor differentiation of Treg cells (Figures S7R–S7T). Based on these data, we conclude that lenalidomide bypasses the CD28 requirement for T cell activation and PD-1 immunotherapy by up-regulating expression of IL-2 and Notch-activated genes.

DISCUSSION

We propose that IKZF1 and IKZF3 suppress expression of IL-2 and Notch targets, both downstream of CD28 co-stimulatory signaling in T cells (Mitra et al., 2020; Powell et al., 1998). Lenalidomide hijacks the CRL4^{CRBN} ubiquitin ligase to degrade these two lymphoid transcription factors, bypassing the CD28 requirement for T cell activation and PD-1 immunotherapy. Ligation of PD-L1 to PD-1 on T cells leads to dephosphorylation of CD28 and inhibition of CD28 downstream signaling (Hui et al., 2017). One of the major effects of PD-1/PD-L1 blockade is activation of inhibition of CD28 downstream signaling, explaining the requirement of CD28 for effective PD-1-targeted therapies (Kamphorst et al., 2017). In mature CD4$^+$ T cells, CD28 signaling elevates Notch ligand expression (Mitra et al., 2020). Notch activation potentiates phosphatidylinositol 3-kinase (PI3K)-dependent signaling downstream of CD28, lowering the activation threshold of CD4$^+$ T cells (Laky et al., 2015). Here we demonstrated that lenalidomide increased expression of IL-2 and augmented Notch signaling to rescue PD-1 blockade efficacy compromised by loss of CD28. IKZF1 represses Notch-activated genes by interacting with recombination signal binding protein for immunoglobulin kappa J region (RBPJ), which forms a complex with intracellular Notch (ICN) to initiate target transcription (Geimer Le Lay et al., 2014). Lenalidomide-induced degradation of IKZF1 therefore might facilitate formation of the Notch transcription complex to activate Notch signaling in T cells. Formation of the complex in T cells can also be enhanced by elevated expression of Notch ligands from other cells, like dendritic cells. Notch Delta-like and Jagged ligands expressed in dendritic cells are critical for T cell-mediated anti-tumor immunity (Tchekneva et al., 2019). It will be interesting to determine the role of dendritic cells in lenalidomide-induced T cell activation and anti-tumor activity using the *Crbn*^{I391V} mouse model in the future.

We reported that most of the tumor-infiltrating CD8$^+$ T cells lost CD28 expression in elderly individuals with CRC, confirming a previous finding in NSCLC (Kamphorst et al., 2017). Here we genetically deleted CD28 in mice to mimic the loss of CD28 expression prevalent in intratumoral T cells from senior individuals with CRC. We found that lenalidomide treatment completely reinstated the PD-1 immunotherapy compromised by CD28 deficiency by engaging humanized Crbn^{I391V} but not WT Crbn in the mouse model. Avadomide, a lenalidomide analog, similarly sensitizes CLL models to PD-1 blockers in mice (Ioannou et al., 2021). Therefore, it will be exciting to clinically test lenalidomide or its analogs as an adjuvant therapy to PD-1/PD-L1 immunotherapy to treat senior individuals with CRC and other solid tumors.

Lenalidomide by itself exhibits very limited anti-tumor activity against solid tumors in the clinic (Semeraro et al., 2013). As a single-agent therapy, lenalidomide treatment produced a partial response in only a small percentage of enrolled individuals with NSCLC and brain tumors (Miller et al., 2007; Warren et al., 2011). In another study, lenalidomide slowed down metastatic tumor progression in a few individuals, especially those with prostate cancer (Dahut et al., 2009). Despite documented evidence that lenalidomide affects circulating T cells, NK cells, and macrophages in affected individuals (Berg et al., 2011; Semeraro et al., 2013), it is impossible to assess the contribution of its immunomodulatory activity to its clinical anti-tumor efficacy. Here we demonstrated that lenalidomide directly activated tumor-infiltrating cytotoxic T lymphocytes (CTLs) to inhibit lenalidomide-insensitive MC38-OVA tumor growth, suggesting that the immunomodulatory rather than the anti-proliferative activity of the drug accounts for its clinical efficacy. However, lenalidomide failed to suppress B16F10 melanoma or 3LL lung adenocarcinoma syngeneic tumor growth in *Crbn*^{I391V} mice, reminiscent of its overall poor clinical effectiveness in solid tumors (Dahut et al., 2009; Miller et al., 2007; Warren et al., 2011). Mechanistically, lenalidomide did not promote activation of peripheral CD8$^+$ T cells or enhance the cytotoxicity of tumor-infiltrating CD8$^+$ T cells in the B16F10-OVA model, which might be due to the overall poor immunogenicity of this tumor model (Kuai et al., 2017). Although 3LL tumors were infiltrated with abundant CD45$^+$ immune cells, most of these cells were CD11b$^+$ myeloid cells, which might form an immune-suppressive microenvironment. The *Crbn*^{I391V} mouse model thus provides us a tool to identify tumor-intrinsic and tumor microenvironment cues that dictate cancer sensitivity to lenalidomide-activated T cells, which will help with selection of individuals most likely to respond to the drug as a single-agent or adjuvant therapy.

Lenalidomide and its analogs directly inhibit proliferation of several B cell malignancies by degradation of essential IKZF1 and IKZF3 proteins (Gao et al., 2020; Kronke et al., 2014, 2015; Lu et al., 2014; Matyskiela et al., 2016; Surka et al., 2020).

CC-90009 also degrades the translation termination factor GSPT1 to induce apoptosis and is in a clinical trial for treating acute myeloid leukemia (Surka et al., 2020). CC-122 can directly kill diffuse large B cell lymphoma (DLBCL) cells by stimulating INF-independent transcription of IFN-stimulated genes (Hagner et al., 2015) and indirectly sensitize CLL cells to PD-1 immunotherapy by triggering the IFN response in T cells (Ioannou et al., 2021). Clinical benefits of such drugs would represent the collective output of their anti-neoplastic activity and CTL stimulation. Such bifunctional molecular glue degraders target the same or distinct neo-substrates in cancer cells and immune cells to deliver a therapeutic index typically achieved by combination therapies of targeted and immunotherapies.

Limitations of this study

There are two major limitations. First, this study does not exclude mechanisms other than IKZF1 and IKZF3 degradation that account for lenalidomide-induced co-stimulation of T cell activation and proliferation. Increased expression of *IL2* and Notch targets can be caused by depletion of other neo-targets, such as ZFP91, after lenalidomide treatment. Second, this study does not provide justification for selecting individuals with cancer most likely to benefit from combination therapy with lenalidomide and PD-1-blocking antibodies. With the limited number of samples from affected individuals examined in this work, lenalidomide reinstates the response of $CD28^{-}$ $CD8^{+}$ T cells isolated from CRC but not NSCLC to PD-1 blockade.

Significance

CD28 co-stimulation signaling is required for PD-1 blockade immunotherapy. We demonstrate that the approved drug lenalidomide targets the $CRL4^{CRBN}$ ubiquitin ligase to activate the Notch and interleukin- 2 pathways in tumor-infiltrating $CD8^{+}$ T cells. These T cells respond to PD-1-blocking antibodies even in the absence of the CD28 co-stimulatory receptor after treatment with lenalidomide. Our results suggest that lenalidomide can clinically enhance PD-1 therapy efficacy when treating solid tumors infiltrated with abundant $CD28^{-}$ $CD8^{+}$ T cells. Our study indicates that molecular glue degraders, such as lenalidomide and pomalidomide, and some other degraders whose substrates, including IKZF1 and IKZF3, will benefit individuals with cancer not only by killing cancer cells directly but also by promoting T cell-based immunotherapy. We propose that the $Crbn^{I391V}$ mouse model is an optimal tool to evaluate the therapeutic significance of lenalidomide and some other molecular glue degraders in the context of cancer immunotherapy.

STAR★METHODS

Detailed methods are provided in the online version of this paper and include the following:

SUPPLEMENTAL INFORMATION

Supplemental information can be found online at https://doi.org/10.1016/j.chembiol.2022.05.012.

ACKNOWLEDGMENTS

We thank H.P. Wang at SHTU for OT-1 and $Cd28^{-/-}$ mice; B. Sun at SIBCB for CD45.1 mice; OIU of WuXi AppTec for technical support; the Nuclear Magnetic Resonance System, Electron Microscopy System, Mass Spectrometry System, Integrated Laser Microscopy System, Molecular Imaging System, Animal Facility, and Database and Computation System at the National Facility for Protein Science in Shanghai (NFPS); the Zhangjiang Lab, Shanghai Advanced Research Institute, Chinese Academy of Science for mouse breeding support; and the Molecular Imaging Core Facility (MICF) and the MCB Core Facility at the School of Life Science and Technology, ShanghaiTech University for providing technical support. This research was supported by Shanghai Frontiers Science Center for Biomacromolecules and Precision Medicine at ShanghaiTech University. The work was supported by the National Natural Science Foundation of China (31970671, 31671334, and 82003803) and Shanghai Science and Technology Commission (18JC1413900).

AUTHOR CONTRIBUTIONS

C.-L.G. and Y.C. conceived the study. C.-L.G. and J.-Y.C. performed most of the experiments. T.-Y.S. contributed to confirmation of IMiD-induced substrate degradation in $Crbn^{I391V}$ mouse cells. J.H.J. contributed to evaluation of lenalidomide effects in CRC samples. M.L. contributed to establishment of MC38-OVA and B16F10-OVA cells and provided technical support. M.-F.S. contributed to analysis and visualization of RNA-seq data. T.J., J.-Y.C., Y.-S.P., B.P., and H.-J.F. contributed to breeding of the $Crbn^{I391V}$ mice and provided technical assistance. B.S.M. and J.G.L. contributed to collection of CRC samples. P.H. contributed to the mass spectrum of $CD8^{+}$ T cells. Q.Z. contributed to data analysis and integration. C.-L.G., E.-C.S., and Y.C. wrote the manuscript. Y.C. obtained funding and supervised the study.

DECLARATION OF INTERESTS

The authors declare no competing interests.

Received: September 30, 2021
Revised: March 24, 2022
Accepted: May 26, 2022
Published: June 21, 2022

REFERENCES

An, J., Ponthier, C.M., Sack, R., Seebacher, J., Stadler, M.B., Donovan, K.A., and Fischer, E.S. (2017). pSILAC mass spectrometry reveals ZFP91 as IMiD-dependent substrate of the CRL4(CRBN) ubiquitin ligase. Nat. Commun. *8*, 15398. https://doi.org/10.1038/ncomms15398.

Aue, G., Sun, C., Liu, D., Park, J.-H., Pittaluga, S., Tian, X., Lee, E., Soto, S., Valdez, J., Maric, I., et al. (2018). Activation of Th1 immunity within the tumor microenvironment is associated with clinical response to lenalidomide in chronic lymphocytic leukemia. J. Immunol. *201*, 1967–1974. https://doi.org/10.4049/jimmunol.1800570.

Bandyopadhyay, S., Dure, M., Paroder, M., Soto-Nieves, N., Puga, I., and Macian, F. (2007). Interleukin 2 gene transcription is regulated by Ikaros-induced changes in histone acetylation in anergic T cells. Blood *109*, 2878–2886. https://doi.org/10.1182/blood-2006-07-037754.

Bartlett, J.B., Dredge, K., and Dalgleish, A.G. (2004). The evolution of thalidomide and its IMiD derivatives as anticancer agents. Nat. Rev. Cancer *4*, 314–322. https://doi.org/10.1038/nrc1323.

Berg, S.L., Cairo, M.S., Russell, H., Ayello, J., Ingle, A.M., Lau, H., Chen, N., Adamson, P.C., and Blaney, S.M. (2011). Safety, pharmacokinetics, and immunomodulatory effects of lenalidomide in children and adolescents with relapsed/refractory solid tumors or myelodysplastic syndrome: a Children's Oncology Group Phase I Consortium report. J. Clin. Oncol. *29*, 316–323. https://doi.org/10.1200/jco.2010.30.8387.

Besson, L., Charrier, E., Karlin, L., Allatif, O., Marçais, A., Rouzaire, P., Belmont, L., Attal, M., Lombard, C., Salles, G., et al. (2018). One-year follow-up of natural killer cell activity in multiple myeloma patients treated with adjuvant lenalidomide therapy. Front. Immunol. *9*, 704. https://doi.org/10.3389/fimmu.2018.00704.

Boon, T., Cerottini, J.C., Van den Eynde, B., van der Bruggen, P., and Van Pel, A. (1994). Tumor antigens recognized by T lymphocytes. Annu. Rev. Immunol. *12*, 337–365. https://doi.org/10.1146/annurev.iy.12.040194.002005.

Chamberlain, P.P., Lopez-Girona, A., Miller, K., Carmel, G., Pagarigan, B., Chie-Leon, B., Rychak, E., Corral, L.G., Ren, Y.J., Wang, M., et al. (2014). Structure of the human Cereblon-DDB1-lenalidomide complex reveals basis for responsiveness to thalidomide analogs. Nat. Struct. Mol. Biol. *21*, 803–809. https://doi.org/10.1038/nsmb.2874.

Chanan-Khan, A.A., Zaritskey, A., Egyed, M., Vokurka, S., Semochkin, S., Schuh, A., Kassis, J., Simpson, D., Zhang, J., Purse, B., and Foà, R. (2017). Lenalidomide maintenance therapy in previously treated chronic lymphocytic leukaemia (CONTINUUM): a randomised, double-blind, placebo-controlled, phase 3 trial. Lancet Haematol. *4*, e534–e543. https://doi.org/10.1016/s2352-3026(17)30168-0.

Chen, D.S., and Mellman, I. (2013). Oncology meets immunology: the cancer-immunity cycle. Immunity *39*, 1–10. https://doi.org/10.1016/j.immuni.2013.07.012.

Cheng, J.W., Duan, L.X., Yu, Y., Wang, P., Feng, J.L., Feng, G.Z., and Liu, Y. (2021). Bone marrow mesenchymal stem cells promote prostate cancer cell stemness via cell-cell contact to activate the Jagged1/Notch1 pathway. Cell Biosci. *11*, 87. https://doi.org/10.1186/s13578-021-00599-0.

Dahut, W.L., Aragon-Ching, J.B., Woo, S., Tohnya, T.M., Gulley, J.L., Arlen, P.M., Wright, J.J., Ventiz, J., and Figg, W.D. (2009). Phase I study of oral lenalidomide in patients with refractory metastatic cancer. J. Clin. Pharmacol. *49*, 650–660. https://doi.org/10.1177/0091270009335001.

Di, J., Liu, M., Fan, Y., Gao, P., Wang, Z., Jiang, B., and Su, X. (2020). Phenotype molding of T cells in colorectal cancer by single-cell analysis. Int. J. Cancer *146*, 2281–2295. https://doi.org/10.1002/ijc.32856.

Dunn, G.P., Old, L.J., and Schreiber, R.D. (2004). The three Es of cancer immunoediting. Annu. Rev. Immunol. *22*, 329–360. https://doi.org/10.1146/annurev.immunol.22.012703.104803.

Esensten, J.H., Helou, Y.A., Chopra, G., Weiss, A., and Bluestone, J.A. (2016). CD28 costimulation: from mechanism to therapy. Immunity *44*, 973–988. https://doi.org/10.1016/j.immuni.2016.04.020.

Filaci, G., Fenoglio, D., Fravega, M., Ansaldo, G., Borgonovo, G., Traverso, P., Villaggio, B., Ferrera, A., Kunkl, A., Rizzi, M., et al. (2007). CD8+ CD28- T regulatory lymphocytes inhibiting T cell proliferative and cytotoxic functions infiltrate human cancers. J. Immunol. *179*, 4323–4334. https://doi.org/10.4049/jimmunol.179.7.4323.

Fink, A.M., Bahlo, J., Robrecht, S., Al-Sawaf, O., Aldaoud, A., Hebart, H., Jentsch-Ullrich, K., Dörfel, S., Fischer, K., Wendtner, C.-M., et al. (2017). Lenalidomide maintenance after first-line therapy for high-risk chronic lymphocytic leukaemia (CLLM1): final results from a randomised, double-blind, phase 3 study. Lancet Haematol. *4*, e475–e486. https://doi.org/10.1016/s2352-3026(17)30171-0.

Fink, E.C., McConkey, M., Adams, D.N., Haldar, S.D., Kennedy, J.A., Guirguis, A.A., Udeshi, N.D., Mani, D.R., Chen, M., Liddicoat, B., et al. (2018). Crbn (I391V) is sufficient to confer in vivo sensitivity to thalidomide and its derivatives in mice. Blood *132*, 1535–1544. https://doi.org/10.1182/blood-2018-05-852798.

Gandhi, A.K., Kang, J., Havens, C.G., Conklin, T., Ning, Y., Wu, L., Ito, T., Ando, H., Waldman, M.F., Thakurta, A., et al. (2014). Immunomodulatory agents lenalidomide and pomalidomide co-stimulate T cells by inducing degradation of T cell repressors Ikaros and Aiolos via modulation of the E3 ubiquitin ligase complex $CRL4^{CRBN}$. Br. J. Haematol. *164*, 811–821. https://doi.org/10.1111/bjh.12708.

Gao, S., Wang, S., and Song, Y. (2020). Novel immunomodulatory drugs and neo-substrates. Biomark. Res. *8*, 2. https://doi.org/10.1186/s40364-020-0182-y.

Geimer Le Lay, A.S., Oravecz, A., Mastio, J., Jung, C., Marchal, P., Ebel, C., Dembélé, D., Jost, B., Le Gras, S., Thibault, C., et al. (2014). The tumor suppressor Ikaros shapes the repertoire of notch target genes in T cells. Sci. Signal. *7*, ra28. https://doi.org/10.1126/scisignal.2004545.

Gemechu, Y., Millrine, D., Hashimoto, S., Prakash, J., Sanchenkova, K., Metwally, H., Gyanu, P., Kang, S., and Kishimoto, T. (2018). Humanized cereblon mice revealed two distinct therapeutic pathways of immunomodulatory drugs. Proc. Natl. Acad. Sci. U S A *115*, 11802–11807. https://doi.org/10.1073/pnas.1814446115.

Görgün, G., Samur, M.K., Cowens, K.B., Paula, S., Bianchi, G., Anderson, J.E., White, R.E., Singh, A., Ohguchi, H., Suzuki, R., et al. (2015). Lenalidomide enhances immune checkpoint blockade-induced immune response in multiple myeloma. Clin. Cancer Res. *21*, 4607–4618. https://doi.org/10.1158/1078-0432.ccr-15-0200.

Hagner, P.R., Man, H.W., Fontanillo, C., Wang, M., Couto, S., Breider, M., Bjorklund, C., Havens, C.G., Lu, G., Rychak, E., et al. (2015). CC-122, a pleiotropic pathway modifier, mimics an interferon response and has antitumor activity in DLBCL. Blood *126*, 779–789. https://doi.org/10.1182/blood-2015-02-628669.

Haslett, P.A., Corral, L.G., Albert, M., and Kaplan, G. (1998). Thalidomide costimulates primary human T lymphocytes, preferentially inducing proliferation, cytokine production, and cytotoxic responses in the CD8+ subset. J. Exp. Med. *187*, 1885–1892. https://doi.org/10.1084/jem.187.11.1885.

Hui, E., Cheung, J., Zhu, J., Su, X., Taylor, M.J., Wallweber, H.A., Sasmal, D.K., Huang, J., Kim, J.M., Mellman, I., and Vale, R.D. (2017). T cell costimulatory receptor CD28 is a primary target for PD-1-mediated inhibition. Science *355*, 1428–1433. https://doi.org/10.1126/science.aaf1292.

Ioannou, N., Hagner, P.R., Stokes, M., Gandhi, A.K., Apollonio, B., Fanous, M., Papazoglou, D., Sutton, L.A., Rosenquist, R., Amini, R.M., et al. (2021). Triggering interferon signaling in T cells with avadomide sensitizes CLL to anti-PD-L1/PD-1 immunotherapy. Blood *137*, 216–231. https://doi.org/10.1182/blood.2020006073.

Jenkins, M.K., Ashwell, J.D., and Schwartz, R.H. (1988). Allogeneic non-T spleen cells restore the responsiveness of normal T cell clones stimulated with antigen and chemically modified antigen-presenting cells. J. Immunol. *140*, 3324–3330.

Kakuda, S., LoPilato, R.K., Ito, A., and Haltiwanger, R.S. (2020). Canonical Notch ligands and Fringes have distinct effects on NOTCH1 and NOTCH2. J. Biol. Chem. *295*, 14710–14722. https://doi.org/10.1074/jbc.ra120.014407.

Kamphorst, A.O., Wieland, A., Nasti, T., Yang, S., Zhang, R., Barber, D.L., Konieczny, B.T., Daugherty, C.Z., Koenig, L., Yu, K., et al. (2017). Rescue of

exhausted CD8 T cells by PD-1-targeted therapies is CD28-dependent. Science *355*, 1423–1427. https://doi.org/10.1126/science.aaf0683.

Kim, K.H., Kim, H.K., Kim, H.D., Kim, C.G., Lee, H., Han, J.W., Choi, S.J., Jeong, S., Jeon, M., Kim, H., et al. (2020). PD-1 blockade-unresponsive human tumor-infiltrating CD8(+) T cells are marked by loss of CD28 expression and rescued by IL-15. Cell. Mol. Immunol. *18*, 385–397.

Krämer, I., Engelhardt, M., Fichtner, S., Neuber, B., Medenhoff, S., Bertsch, U., Hillengass, J., Raab, M.S., Hose, D., Ho, A.D., et al. (2016). Lenalidomide enhances myeloma-specific T-cell responses in vivo and in vitro. OncoImmunology *5*, e1139662. https://doi.org/10.1080/2162402x.2016.1139662.

Kronke, J., Fink, E.C., Hollenbach, P.W., MacBeth, K.J., Hurst, S.N., Udeshi, N.D., Chamberlain, P.P., Mani, D.R., Man, H.W., Gandhi, A.K., et al. (2015). Lenalidomide induces ubiquitination and degradation of CK1α in del(5q) MDS. Nature *523*, 183–188. https://doi.org/10.1038/nature14610.

Krönke, J., Udeshi, N.D., Narla, A., Grauman, P., Hurst, S.N., McConkey, M., Svinkina, T., Heckl, D., Comer, E., Li, X., et al. (2014). Lenalidomide causes selective degradation of IKZF1 and IKZF3 in multiple myeloma cells. Science *343*, 301–305. https://doi.org/10.1126/science.1244851.

Kuai, R., Ochyl, L.J., Bahjat, K.S., Schwendeman, A., and Moon, J.J. (2017). Designer vaccine nanodiscs for personalized cancer immunotherapy. Nat. Mater. *16*, 489–496. https://doi.org/10.1038/nmat4822.

Lagrue, K., Carisey, A., Morgan, D.J., Chopra, R., and Davis, D.M. (2015). Lenalidomide augments actin remodeling and lowers NK-cell activation thresholds. Blood *126*, 50–60. https://doi.org/10.1182/blood-2015-01-625004.

Laky, K., Evans, S., Perez-Diez, A., and Fowlkes, B.J. (2015). Notch signaling regulates antigen sensitivity of naive CD4+ T cells by tuning co-stimulation. Immunity *42*, 80–94. https://doi.org/10.1016/j.immuni.2014.12.027.

Lapenta, C., Donati, S., Spadaro, F., Lattanzi, L., Urbani, F., Macchia, I., Sestili, P., Spada, M., Cox, M.C., Belardelli, F., and Santini, S.M. (2019). Lenalidomide improves the therapeutic effect of an interferon-alpha-dendritic cell-based lymphoma vaccine. Cancer Immunol. Immunother. *68*, 1791–1804. https://doi.org/10.1007/s00262-019-02411-y.

LeBlanc, R., Hideshima, T., Catley, L.P., Shringarpure, R., Burger, R., Mitsiades, N., Mitsiades, C., Cheema, P., Chauhan, D., Richardson, P.G., et al. (2004). Immunomodulatory drug costimulates T cells via the B7-CD28 pathway. Blood *103*, 1787–1790. https://doi.org/10.1182/blood-2003-02-0361.

Lu, G., Middleton, R.E., Sun, H.H., Naniong, M., Ott, C.J., Mitsiades, C.S., Wong, K.K., Bradner, J.E., and Kaelin, W.G. (2014). The myeloma drug lenalidomide promotes the cereblon-dependent destruction of Ikaros proteins. Science *343*, 305–309. https://doi.org/10.1126/science.1244917.

Matyskiela, M.E., Lu, G., Ito, T., Pagarigan, B., Lu, C.-C., Miller, K., Fang, W., Wang, N.-Y., Nguyen, D., Houston, J., et al. (2016). A novel cereblon modulator recruits GSPT1 to the CRL4CRBN ubiquitin ligase. Nature *535*, 252–257. https://doi.org/10.1038/nature18611.

Matyskiela, M.E., Zhang, W., Man, H.W., Muller, G., Khambatta, G., Baculi, F., Hickman, M., LeBrun, L., Pagarigan, B., Carmel, G., et al. (2018). A cereblon modulator (CC-220) with improved degradation of Ikaros and aiolos. J. Med. Chem. *61*, 535–542. https://doi.org/10.1021/acs.jmedchem.6b01921.

Ménard, C., Rossille, D., Dulong, J., Nguyen, T.T., Papa, I., Latour, M., Bescher, N., Bezier, I., Chouteau, M., Fest, T., et al. (2021). Lenalidomide triggers T-cell effector functions in vivo in patients with follicular lymphoma. Blood Adv. *5*, 2063–2074. https://doi.org/10.1182/bloodadvances.2020003774.

Miller, A.A., Case, D., Harmon, M., Savage, P., Lesser, G., Hurd, D., and Melin, S.A. (2007). Phase I study of lenalidomide in solid tumors. J. Thorac. Oncol. *2*, 445–449. https://doi.org/10.1097/01.jto.0000268679.33238.67.

Mitra, A., Shanthalingam, S., Sherman, H.L., Singh, K., Canakci, M., Torres, J.A., Lawlor, R., Ran, Y., Golde, T.E., Miele, L., et al. (2020). CD28 signaling drives notch ligand expression on CD4 T cells. Front. Immunol. *11*, 735. https://doi.org/10.3389/fimmu.2020.00735.

Palma, M., Hansson, L., Mulder, T.A., Adamson, L., Näsman-Glaser, B., Eriksson, I., Heimersson, K., Ryblom, H., Mozaffari, F., Svensson, A., et al. (2018). Lenalidomide as immune adjuvant to a dendritic cell vaccine in chronic lymphocytic leukemia patients. Eur. J. Haematol. *101*, 68–77. https://doi.org/10.1111/ejh.13065.

Paolini, A., Fontana, F., Pham, V.C., Rödel, C.J., and Abdelilah-Seyfried, S. (2021). Mechanosensitive Notch-Dll4 and Klf2-Wnt9 signaling pathways intersect in guiding valvulogenesis in zebrafish. Cell Rep. *37*, 109782. https://doi.org/10.1016/j.celrep.2021.109782.

Powell, J.D., Ragheb, J.A., Kitagawa-Sakakida, S., and Schwartz, R.H. (1998). Molecular regulation of interleukin-2 expression by CD28 co-stimulation and anergy. Immunol. Rev. *165*, 287–300. https://doi.org/10.1111/j.1600-065x.1998.tb01246.x.

Quintana, F.J., Jin, H., Burns, E.J., Nadeau, M., Yeste, A., Kumar, D., Rangachari, M., Zhu, C., Xiao, S., Seavitt, J., et al. (2012). Aiolos promotes TH17 differentiation by directly silencing Il2 expression. Nat. Immunol. *13*, 770–777. https://doi.org/10.1038/ni.2363.

Semeraro, M., Vacchelli, E., Eggermont, A., Galon, J., Zitvogel, L., Kroemer, G., and Galluzzi, L. (2013). Trial watch: lenalidomide-based immunochemotherapy. OncoImmunology *2*, e26494. https://doi.org/10.4161/onci.26494.

Subramanian, A., Tamayo, P., Mootha, V.K., Mukherjee, S., Ebert, B.L., Gillette, M.A., Paulovich, A., Pomeroy, S.L., Golub, T.R., Lander, E.S., and Mesirov, J.P. (2005). Gene set enrichment analysis: a knowledge-based approach for interpreting genome-wide expression profiles. Proc. Natl. Acad. Sci. U S A *102*, 15545–15550. https://doi.org/10.1073/pnas.0506580102.

Surka, C., Jin, L., Mbong, N., Lu, C.C., Jang, I.S., Rychak, E., Mendy, D., Clayton, T., Tindall, E.A., Hsu, C., et al. (2020). CC-90009, a novel cereblon E3 ligase modulator targets acute myeloid leukemia blasts and leukemia stem cells. Blood *137*, 661–677.

Tchekneva, E.E., Goruganthu, M.U.L., Uzhachenko, R.V., Thomas, P.L., Antonucci, A., Chekneva, I., Koenig, M., Piao, L., Akhter, A., de Aquino, M.T.P., et al. (2019). Determinant roles of dendritic cell-expressed Notch Delta-like and Jagged ligands on anti-tumor T cell immunity. J. Immunother. Cancer *7*, 95. https://doi.org/10.1186/s40425-019-0566-4.

Wang, X., Walter, M., Urak, R., Weng, L., Huynh, C., Lim, L., Wong, C.W., Chang, W.C., Thomas, S.H., Sanchez, J.F., et al. (2018). Lenalidomide enhances the function of CS1 chimeric antigen receptor-redirected T cells against multiple myeloma. Clin. Cancer Res. *24*, 106–119. https://doi.org/10.1158/1078-0432.ccr-17-0344.

Warren, K.E., Goldman, S., Pollack, I.F., Fangusaro, J., Schaiquevich, P., Stewart, C.F., Wallace, D., Blaney, S.M., Packer, R., Macdonald, T., et al. (2011). Phase I trial of lenalidomide in pediatric patients with recurrent, refractory, or progressive primary CNS tumors: pediatric Brain Tumor Consortium study PBTC-018. J. Clin. Oncol. *29*, 324–329. https://doi.org/10.1200/jco.2010.31.3601.

Weng, N.P., Akbar, A.N., and Goronzy, J. (2009). CD28(-) T cells: their role in the age-associated decline of immune function. Trends Immunol. *30*, 306–312. https://doi.org/10.1016/j.it.2009.03.013.

Witzig, T.E., Nowakowski, G.S., Habermann, T.M., Goy, A., Hernandez-Ilizaliturri, F.J., Chiappella, A., Vitolo, U., Fowler, N., and Czuczman, M.S. (2015). A comprehensive review of lenalidomide therapy for B-cell non-Hodgkin lymphoma. Ann. Oncol. *26*, 1667–1677. https://doi.org/10.1093/annonc/mdv102.

STAR★METHODS

KEY RESOURCES TABLE

REAGENT or RESOURCE	SOURCE	IDENTIFIER
Antibodies		
Ikaros Antibody	Cell Signaling Technology	Cat# 5443; RRID: AB_10691693
Aiolos Rabbit mAb	Cell Signaling Technology	Cat# 15103; RRID: AB_2744524
β-Actin Rabbit mAb	Cell Signaling Technology	Cat# 4970; RRID: AB_2223172
Anti-CRBN Antibody	Sigma	Cat# HPA045910; RRID: 10960409
Anti-ZFP91 Antibody	Bethyl Laboratories	Cat# A303-245A; RRID: AB_10953803
Anti-mouse CD3e antibody	BD Biosciences	Cat# 550275; RRID: AB_393572
Anti-mouse CD28 antibody	BD Biosciences	Cat# 553294; RRID: AB_394763
Anti-mouse IL2 antibody	Bio X cell	Cat# BE0042; RRID: AB_1107703
Anti-mouse CD4 antibody	Bio X cell	Cat# BE0119; RRID: AB_10950382
Anti-mouse CD8 antibody	Bio X cell	Cat# BE0117; RRID: AB_10950145
Anti-mouse PD-1 antibody	Bio X cell	Cat# BE0146; RRID: AB_10949053
Anti-human CD3 antibody	Miltenyi Biotec	Cat# 130-093-387; RRID: AB_1036144
Anti-human PD-1 antibody	BioLegend	Cat# 329946; RRID: AB_2566290
Purified rat anti-mouse CD16/CD32	BD Biosciences	Cat# 553142; RRID: AB_394656
PerCP-Cy5.5 anti-mouse CD4	BD Biosciences	Cat# 550954; RRID: AB_393977
BV510 anti-mouse CD8	BD Biosciences	Cat# 563068; RRID: AB_2687548
AF488 anti-mouse Aiolos	BD Biosciences	Cat# 565266; RRID: AB_2739141
APC anti-mouse CD279	BD Biosciences	Cat# 562671; RRID: AB_2737712
PE anti-mouse IFNγ	BD Biosciences	Cat# 554412; RRID: AB_395376
BV605 anti-mouse CD25	BD Biosciences	Cat# 563061; RRID: AB_2737982
APC-Cy7 anti-human CD8	BD Biosciences	Cat# 560179; RRID: AB_1645481
FITC anti-human CD28	BD Biosciences	Cat# 564492; RRID: AB_2744355
BV711 anti-human CD25	BD Biosciences	Cat# 563159; RRID: AB_2738037
PE-Cy7 anti-human CD69	BD Biosciences	Cat# 557745; RRID: AB_396851
Alexa Fluor 647 anti-Ki-67	BD Biosciences	Cat# 558615; RRID: AB_647130
BV510 anti-mouse CD11b	BD Biosciences	Cat# 562950; RRID: AB_2737913
AF700 anti-mouse CD45	BioLegend	Cat# 147716; RRID: AB_2750449
FITC anti-mouse LAG-3	BioLegend	Cat# 369308; RRID: AB_2629751
AF647 anti-mouse Granzyme B	BioLegend	Cat# 515406; RRID: AB_2566333
PE anti-mouse T-bet	BioLegend	Cat# 644809; RRID: AB_2028583
APC-Cy7 anti-mouse CD279	BioLegend	Cat# 135223; RRID: AB_2563522
BV605 anti-mouse CD44	BioLegend	Cat# 103047; RRID: AB_2562451
PE anti-mouse Ikaros	BioLegend	Cat# 653304; RRID: AB_2561728
PE anti-mouse CD69	BioLegend	Cat# 104508; RRID: AB_313111
AF647 anti-mouse Ki-67	BioLegend	Cat# 652408; RRID: AB_2562139
APC anti-mouse CD28	BioLegend	Cat# 102110; RRID: AB_312875
PE anti-mouse CD19 antibody	BioLegend	Cat# 115507; RRID: AB_313642
PE-Cy7 anti-mouse FoxP3	eBioscience	Cat# 25-5773-82; RRID: AB_891552
PE anti-mouse TIM-3	eBioscience	Cat# 12-5870-82; RRID: AB_465974
Bacterial and virus strains		
DH5α Competent Cells	Yeasen	11802ES80
Lentivirus	This paper	N/A

(*Continued on next page*)

Continued

REAGENT or RESOURCE	SOURCE	IDENTIFIER
Biological samples		
Human PBMC samples	Yonsei Cancer Center; Republic of Korea	N/A
Human colorectal cancer tissue	Yonsei Cancer Center; Republic of Korea	N/A
Human non-small-cell lung cancer tissue	Severance Hospital; Republic of Korea	N/A
Chemicals, peptides, and recombinant proteins		
Lenalidomide	Selleck	Cat# S1029
Thalidomide	Selleck	Cat# S1193
Pomalidomide	Selleck	Cat# S1567
CC122	Selleck	Cat# S7892
CC220	Selleck	Cat# S8760
rmDll1	R&D SYSTEMS	Cat# 5026-DL-050
Recombinant Murine IL-2	Peprotech	Cat# 212-12
Critical commercial assays		
EasySep Mouse $CD8^+$ T Cell Isolation Kit	STEMCELL Technologies	Cat# 19853
EasySep Mouse $CD4^+$ T Cell Isolation Kit	STEMCELL Technologies	Cat# 19852
Mouse IFNγ Quantikine ELISA Kit	R&D SYSTEMS	Cat# MIF00
Mouse IL-2 Quantikine ELISA Kit	R&D SYSTEMS	Cat# M2000
Cell Counting Kit (CCK8)	Yeasen	Cat# 40203ES60
Foxp3/Transcription Factor Staining Buffer Set	Thermo Fisher	Cat# 00-5523-00
CellTrace CFSE Cell Proliferation Kit	Invitrogen	Cat# C34554
SPARKscritpt II RT Plus Kit	SparkJade	Cat# AG0304
Deposited data		
RNA sequencing data	This paper	Genome Sequence Archive: https://ngdc.cncb.ac.cn/gsa/browse/CRA006006
Experimental models: Cell lines		
MC38	WuXi Apptec.	N/A
B16F10	WuXi Apptec.	N/A
3LL	WuXi Apptec.	N/A
MC38-OVA	This paper	N/A
B16F10-OVA	This paper	N/A
Jurkat	ATCC	Cat# TIB-512
Experimental models: Organisms/strains		
Mouse: *Crbn*^{I391V} C57BL/6 mice	This paper	N/A
Mouse: *Cd28*$^{-/-}$ C57BL/6 mice	Prof. Chenqi Xu's laboratory, School of life science and technology, ShanghaiTech University	N/A
Mouse: OT-1 C57BL/6 mice	Prof. Haopeng Wang's laboratory, School of life science and technology, ShanghaiTech University	N/A
Mouse: Cas9 transgenic C57BL/6 mice	Prof. Tian Chi's laboratory, School of life science and technology, ShanghaiTech University	N/A

(*Continued on next page*)

Continued		
REAGENT or RESOURCE	SOURCE	IDENTIFIER
Oligonucleotides		
Primers for Real-Time PCR, see Table S1	This paper	N/A
Recombinant DNA		
lentiCRISPR v2	Addgene	Cat# 52961
pLenti6/V5/DEST-VPS35	Addgene	Cat# 21691
pCMV-VSV-G	Addgene	Cat# 8454
psPAX2	Addgene	Cat# 12260
OVA cDNA	Genewiz	N/A
Software and algorithms		
GraphPad Prism 8	GraphPad	https://www.graphpad.com/scientific-software/prism/
FlowJo V10	FlowJo	https://www.flowjo.com/solutions/flowjo/downloads
Image Lab 6.0.1	Bio-Rad	https://www.bio-rad.com/en-us/product/image-lab-software?ID=KRE6P5E8Z
RStudio	RStudio	https://www.rstudio.com/download/
SnapGene	SnapGene	https://www.snapgene.com/

RESOURCE AVAILABILITY

Lead contact

Further information and requests for resources and reagents should be directed to and will be fulfilled by the lead contact, Yong Cang (cangyong@shanghaitech.edu.cn).

Materials availability

Any plasmids, cell lines and mouse lines generated in this study are available from the lead contact upon request.

Data and code availability

- RNAseq data have been deposited at Genome Sequence Archive (GSA) and are publicly available as of the date of publication. Accession numbers are listed in the key resources table. All other data reported in this paper will be shared by the lead contact upon request.
- This paper does not report original code.
- Any additional information required to reanalyze the data reported in this paper is available from the lead contact upon request.

EXPERIMENTAL MODEL AND SUBJECT DETAILS

Animals

All mice were on C57BL/6 background. *Cd28*$^{+/+}$ *Crbn*$^{+/+}$, *Cd28*$^{+/+}$ *Crbn*^{I391V}, *Cd28*$^{-/-}$ *Crbn*$^{+/+}$ and *Cd28*$^{-/-}$*Crbn*^{I391V} mice were generated and bred in house. All of these mice were test-naïve and healthy before the *in vivo* study. All experiments were conducted using 6- to 14-week-old mice and only female mice were used. These mice were inoculated subcutaneously with 2 × 10^6 MC38-OVA murine CRC cells or B16F10-OVA murine melanoma cells in PBS. Tumor-bearing mice were randomly assigned to different treatment groups 5 days after inoculation (when the tumor volume reached around 80 mm^3) for MC38-OVA tumors and 4 days after inoculation (when the tumor volume reached around 40 mm^3) for B16F10-OVA tumors. The protocol and any amendment(s) or procedures involving the care and use of animals in this study were in accordance with Shanghai Institutional Animal Care and Use Committee (IACUC) guidelines and approved by IACUC of ShanghaiTech University or WuXi AppTec prior to conduct. Animal experiments were conducted at the National Facility for Protein Science and OIU of WuXi AppTec.

Clinical samples

The CRC and NSCLC specimens were obtained under a protocol approved by the institutional review board of Korea Advanced Institute of Science and Technology (4-2019-0811), and all patients provided written informed consent. The information of CRC and NSCLC patients are listed below.

Information of CRC patients providing PBMC samples.

Patient number	Age	Sex	MSI status	Stage
72	66	M	UK	1
89	60	M	MSS	3
207	71	F	MSS	X
350	63	M	MSS	3
385	77	M	MSS	2
389	37	M	MSS	3
401	69	M	MSS	3
402	41	F	MSS	3
423	64	M	MSS	2

Information of CRC patients providing tumor samples.

Patient number	Age	Sex	MSI status	Stage
395	55	M	MSS	2
403	72	M	MSS	2
411	50	M	MSS	3
448	76	F	MSI-High	1
456	66	M	UK	X
405	54	F	MSI-High	4a
446	53	F	UK	X

Information of NSCLC patients providing tumor samples.

Patient number	Age	Sex	Stage
23	69	M	IIIA
47	65	M	IA2
49	60	F	IB
60	48	F	IA3
67	44	F	IA2
89	54	F	IIIA
94	67	M	IA3

Cell lines

Mouse colon cancer cell line MC38 (derived from female C57BL/6 mouse), mouse melanoma cell line B16F10 (derived from male C57BL/6 mouse) and mouse lung cancer cell line 3LL (the gender information of this cell line is not available) were obtained from WuXi AppTec. MC38-OVA and B16F10-OVA were generated from MC38 and B16F10 in house. Human T cell leukemia cell Jurkat (male) were obtained from ATCC (TIB-152). MC38, MC38-OVA and 3LL cells were maintained in complete DMEM media (Sigma, 10% FBS and 50 U/mL of Penicillin-Streptomycin). B16F10, B16F10-OVA and Jurkat cells were maintained in complete RPMI-1640 media (Sigma, 10% FBS and 50 U/mL of Penicillin-Streptomycin). The cells were maintained in a humidity-controlled environment (37°C, 5% CO_2). The cell lines used in this study have not been authenticated. All cell lines used in this study were tested as Mycoplasma-negative using the Universal Mycoplasma Detection Kit (ATCC, 30-1012K).

Primary cell cultures

Primary T cells were isolated from mouse spleens and both male and female mice were used for T cell isolation. A single-cell suspension of mouse splenocytes was obtained by crushing spleens though a 40-μM cell strainer. $CD4^+$ and $CD8^+$ T cells were isolated from mouse splenocytes using mouse CD4 positive selection kit (Stemcell, # 18952) and mouse CD8a positive selection kit (Stemcell, # 18953) according to the manufacturer's protocol. T cells isolated from mice were cultured in complete RPMI-1640 media (Sigma, 10% HIFBS, 20 mM HEPES, 1 mM sodium pyruvate, 0.05 mM 2-mercaptoethanol, 1X GluMax, 50 U/mL of Penicillin-Streptomycin). The primary T cells were maintained in a humidity-controlled environment (37°C, 5% CO_2).

METHOD DETAILS

Generation of *Crbn*^{I391V} mouse model

Crbn^{I391V} mice were generated via CRISPR-Cas9 system. Candidate intact sgRNAs were amplified from the PX459 plasmid (Addgene, 48139) using T7 promoter tagged primers (Forward: ttaatacgactcactataggNNNNNNNNNNNNNNNNNNN, Reverse: AAAAGCACCGACTCGGTGCC). Transcription was performed by MEGAshortscript T7 kit (Thermo Fisher, AM1354) and the product was purified by MEGAclear kit (Thermo Fisher, AM1908). To test the efficiency of sgRNAs *in vitro*, a short DNA fragment (500 bp) around the targeting site of CRBN was amplified from mouse genomic DNA. Cleavage was performed using Cas9 Nuclease (NEB, #M0646) and purified intact sgRNAs, incubated at 37°C for 1 h sgRNA#1 (TCACGAGAAGCCTAGTACAA) had higher efficiency and was used for Microinjection. The purified sgRNA#1 and Cas9 mRNA that transcribed from PX459 by mMESSAGE mMACHINE T7 Ultra Kit (Thermo Fisher, AM1345) were injected together with an ssDNA "donor" sequence (I391V mutation highlighted in yellow and synonymous mutations highlighted in green, ATCTCACGAGAAGCCTAGTACAAAGGCTAAAAATAGGTTTTAACTTATA TCTTTCCTTCATTTTATAGGTATGCATGGACCGTTGCgCAaTGCAAGATaTGTGCtAGCCAcATTGGATGGAAATTTACAGCCACAAA AAAAGACATGTCACCTCAAAAATTTTGGGGCTTAACTCGCTCTGCTCTGTTAC, 190nt) into C57BL/6 background zygotes. The zygotes were cultured in KSOM medium (Sigma, MR-101-D) at 37°C in a 5% CO_2 incubator until the two-cell stage and then were transplanted into pseudo-pregnant ICR female mice. The off-springs were screened by sequencing. For genotyping, a sequence surrounding the I391V coding exon in *Crbn* was amplified using forward and reverse primers. Forward: GCTGGAGCCAA CAGCAACATA; Reverse: TGGAATTGTGGGTAACAGAGCAG. Age-matched C57BL/6 mice were purchased from Shanghai SLAC Laboratory Animal Co. OT-1, *Cd28*$^{-/-}$ and CD45.1C57BL/6 mice were gifts from Prof. Haopeng Wang (School of Life Science and Technology, ShanghaiTech University, Shanghai, China). *Crbn*^{I391V} mice were bred to OT-1 and *Cd28*$^{-/-}$ mice in house. The protocol and any amendment(s) or procedures involving the care and use of animals in this study were in accordance with Shanghai Institutional Animal Care and Use Committee (IACUC) guidelines and approved by IACUC of ShanghaiTech University or WuXi AppTec prior to conduct. Animal experiments were conducted at the National Facility for Protein Science and OIU of WuXi AppTec.

Generation of MC38-OVA and B16F10-OVA cells

Truncated ovalbumin (OVA) was amplified from synthesized OVA cDNA and cloned into pLenti6/V5/DEST-VPS35 (Addgene, #21691) using directional cloning with BamH1 and Xho1. OVA-expressing vector was co-transfected with packaging plasmids pCMV-VSV-G (Addgene, #8454) and psPAX2 (Addgene, #12260) into 293FT cells. Virus was collected 72 h after transfection, titered and stored at −80°C. MC38 and B16F10 cells were infected with OVA-expressing lentivirus overnight. Infected cells were selected with 5 μg/mL of blasticidin ((Life Technologies, R21001). To get clones with optimal expression of OVA and presentation of OVA peptide (SIINFEKL), MC38-OVA and B16F10-OVA cells were single-cell sorted into 96-well plates. Then the clones were screened using Western Blot to detect the expression of OVA followed by co-culture with OT-1 T cells or WT T cells to determine whether the OVA-expressing clones could induce immune response of OT-1 T cells efficiently and specifically. MC38-OVA clone 31 showed strong expression of OVA and could induce activation of OT-1 T cells efficiently and specifically. B16F10-OVA clone 9 showed modest expression of OVA and could induce activation of OT-1 T cells efficiently and specifically in the presence of IFNγ (5 ng/mL, CST, 39127) pre-treatment. These 2 clones were selected for subsequent *in vitro* and *in vivo* experiments.

T cell isolation and activation assay

A single-cell suspension of mouse splenocytes was obtained by crushing spleens though a 40-μM cell strainer. $CD4^+$ and $CD8^+$ T cells were isolated from mouse splenocytes using mouse CD4 positive selection kit (Stemcell, # 18952) and mouse CD8a positive selection kit (Stemcell, # 18953) according to the manufacturer's protocol. For proliferation assay, isolated T cells were stained with CFSE (Invitrogen, C34554) before lenalidomide (Selleck, S1029), pomalidomide (Selleck, S1567) and thalidomide (Selleck, S1193) treatment. Then compound pre-treated T cells were seeded into 96-well plates that were pre-coated with anti-CD3e (0.2 μg/mL, BD Biosciences, 550275) or anti-CD3e plus anti-CD28 (2 μg/mL, BD Biosciences, 553294) antibody for stimulation. For blocking of IL2, 2 μg/mL anti-mouse IL2 (BioXcell, BE0042) were used during activation assay. For block of Notch signaling, 10 μM RO492 (MCE, HY-11102) or IMR-1 (MCE, HY-100431) were added during T cell activation assay.

OT-1 T cell killing assay

MC38-OVA or B16F10-OVA cells were seeded into 96-well plates one day before co-culture at 2000 cells per well. Freshly isolated WT OT-1 or *Crbn*^{I391V} OT-1 $CD8^+$ T cells were pre-treated with DMSO or lenalidomide for 2 h before being added into the 96-well plates with tumor cells for co-culture. For killing assay of B16F10-OVA cells, B16F10-OVA cells were pulsed with 5 ng/mL IFNγ

(CST, 39127) for 18 h before co-culture. The tumor cells and OT-1 T cells were co-cultured for 2 to 4 days, and T cells were removed by washing with PBS after co-culture. The number of tumor cells after T cell killing were quantified by Cell Counting Kit (CCK8, Yeasen 40203ES60).

In vivo tumor model

Female C57BL/6 mice (6-12w) were inoculated subcutaneously with 2 × 10^6 MC38-OVA murine CRC cells or B16F10-OVA murine melanoma cells in PBS. Mice were randomized into different treatment groups 5 days after inoculation (when the tumor volume reached around 80 mm^3) for MC38-OVA tumors and 4 days after inoculation (when the tumor volume reached around 40 mm^3) for B16F10-OVA tumors. Mice in which tumors exceeded the limits were euthanized and removed from the study. Tumors were measured every day or every other day using a caliper and the tumor volume was calculated by following formula:

$$Volume = length * width * width/2$$

In vivo treatment

The number of mice in each treatment group was determined by power calculation, using the ''Sample size'' and ''stats19'' packages in R program. For depletion of $CD4^+$ and $CD8^+$ T cells, 400μg/injection anti-mouse CD4 (BioXcell, BE0119) and 400μg/injection anti-mouse CD8 (BioXcell, BE0117) were administered by intraperitoneal injection in the first week and T cell depletion was maintained for the duration of the experiment by repeated injections of 200μg/injection of anti-mouse CD4 and anti-mouse CD8 antibodies every week. The mice were euthanized by CO_2 asphyxiation 6–10 days after treatment. The people measuring and harvesting tumors were blinded to treatment group.

Lenalidomide was re-suspended in sterile 0.5% Sodium carboxymethyl cellulose (CMC-Na) at 10 mg/mL. The grouped mice were administered orally with lenalidomide suspension at 50 mg/kg every day.

For block of the PD-1 pathway, anti-mouse PD-1 (BioXcell, BE0146) was administered by intraperitoneal injection at 5 mg/kg every other day. Anti-mouse PD-1 antibody were diluted in sterile PBS.

For block of Notch signaling, the γ-secretase inhibitor RO4929097 (RO492) was dissolved in the recommended vehicle (10% DMSO, 40% PEG, 5% Tween-80, 45% saline) in a recommended procedure at 4 mg/mL. The grouped mice were administered by intraperitoneal injection with RO492 solution at 20 mg/kg daily.

For block of IL2, anti-mouse IL2 (BioXcell, BE0042) was administered by intraperitoneal injection at 500 μg/injection every other day. Anti-mouse IL2 antibody were diluted in sterile PBS.

Flow cytometry

For mouse splenocyte analysis, a single-cell suspension of mouse splenocytes was obtained by crushing spleens though a 70-μM cell strainer. Then the single cell suspensions were incubated with Purified rat anti-mouse CD16/CD32 (BD Biosciences, 553142) and then stained with Fixable Viability Dye eFluor™ 450 (1:1000, Invitrogen, 65-0863-18) and primary antibodies. For TILs analysis, tumors were harvested and cut up on ice followed by incubation in RPMI-1640 (Gibco) supplemented with collagenase D (1 mg/mL, Roche), DNase I (50 μg/mL, Sigma-Aldrich) and Hyaluronidase (100 μg/mL, Sigma-Aldrich) for 30 min at 37°C. After incubation, a single-cell suspension of mouse tumor was obtained by crushing the digested tumor though a 70-μM cell strainer. Then the single cell suspensions were incubated with Purified rat anti-mouse CD16/CD32 and then stained with Fixable Viability Dye eFluor™ 450 (1:1000) and primary antibodies. For staining of intracellular protein, the Foxp3/Transcription Factor Staining Buffer Set (Invitrogen, 00-5523-00) was used. The following conjugated antibodies were used: AF700 anti-CD45 (560510), PerCP-Cy5.5 anti-CD4 (550954), BV510 anti-CD8 (563068), AF488 anti-Aiolos (565266), APC anti-CD279 (562671), PE anti-IFNγ (554412), BV605 anti-CD25 (563061), PE anti-human CD28 (555729), APC-Cy7 anti-human CD8 (560179), FITC anti-human CD28 (564492), BV711 anti-human CD25 (563159), PerCP-Cy5.5 anti-human CD3 (560835), PE-Cy7 anti-human CD69 (557745) and AF700 anti-human CD8 (557945) were purchased from BD Biosciences. FITC anti-LAG-3 (369308), AF647 anti-Granzyme B (515406), PE T-bet (644809), APC-Cy7 anti-CD279(135223), PE anti-Ikaros (653304), PE anti-CD69 (104508), AF647 anti-Ki-67 (652408), BV605 anti-CD44 (103047), APC anti-CD28 (102110), PE-Cy7 anti-CD69 (104512), BV605 anti-human Ki-67 (350522) and PE anti-human PD-1 (329906) were purchased from BioLegend; PE-Cy7 anti-FoxP3 (25-5773-82) and PE anti-TIM-3 (12-5870-82) purchased from eBioscience.

Immunoblot analysis

Cells were lysed at 4°C in RIPA buffer containing EDTA-free protease inhibitor cocktail (Roche, 11836170001). Proteins were quantified with the Pierce BCA Protein Assay Kit (Thermo Fisher). Proteins were separated by SDS-PAGE and transferred onto 0.45μm pore size Immobilon PVDF membrane (Millipore). PVDF membranes were blocked with TBS-T (50 mM Tris, 150 mM NaCl, and 0.1% Tween-20) containing 5% (w/v) milk. Membranes were incubated with primary antibodies followed by TBS-T washes and incubation with HRP-conjugated secondary antibodies. The signal was visualized with Supersignal West Dura Extended Duration Substrate (Pierce) and ChemiDoc Imaging System (Bio-Rad). The following antibodies were used: anti-CRBN (Sigma, HPA045910), anti-Ikaros (CST, 5443), anti-Aiolos (CST, 15103), anti-ZFP91(Bethyl Laboratories, A303-245A), anti-β-Actin (CST, 4970) and HRP-labeled Goat Anti-Rabbit IgG (Epizyme, LF102).

Cellular thermal shift assay

Cellular thermal shift assay (CETSA) was performed as previously described. Briefly, for determination of melting curve, isolated $CD8^+$ T cells were re-suspended at 2 × 10^6 cells/mL followed by incubation with DMSO or 20 μM lenalidomide for 1 h at 37°C. The cells were harvested and re-suspended in 800 μL PBS containing protease inhibitor cocktail and then divided into 7 PCR tubes at 100 μL/tube. The 7 PCR tubes were heated with 7 designated temperatures (47°C, 51°C, 55°C, 57°C, 59°C, 60°C, 61°C) for 3 min respectively. Immediately after heating, remove and incubate the tubes at room temperature for 3 min. After this 3-min incubation, immediately snap-freeze the samples. The collected cells were lysed by Freeze-thaw three times for following immunoblot analysis.

RNA sequencing and analysis

$CD8^+$ T cells were isolated from *Crbn*$^{+/+}$ and *Crbn*^{I391V} mouse spleens followed by indicated treatments for 24 h. For the RNAseq to compare the co-stimulation induced by lenalidomide and anti-CD28, $CD8^+$ T cells were stimulated with 0.2 μg/mL anti-CD3e antibody plus 10 μM lenalidomide or 4 μg/mL anti-CD28 antibody. For the RNAseq to investigate the mechanisms underlying the co-stimulation induced by lenalidomide and pomalidomide, $CD8^+$ T cells were co-stimulated with 10 μM lenalidomide or 1 μM pomalidomide. For the RNAseq to identified the IL2-independent mechanisms underlying lenalidomide-induced co-stimulation, *Crbn*^{I391V} $CD8^+$ T cells were co-stimulated with 2 ng/mL IL2 or 10 μM lenalidomide in the presence or absence of 2 μg/mL IL2 blocking antibody. Then the $CD8^+$ T cells were collected in Trizol LS (Invitrogen) as described. Samples were sent to Mingma Technologies Co., Ltd. for RNA extraction, library construction and sequencing. RNeasy MinElute Cleanup Kit (QIAGEN, 74204) was used for RNA extraction, followed by generating mRNA-focused sequencing libraries from total RNA using Illumina® TruSeq® RNA Sample Preparation Kit v2. Paired-end 150 bp sequencing was done on illumina Hiseq X10 (40 M reads for each sample).

The transcriptomic analysis work flow began with a thorough quality check by FastQC (0.11.2) and the adapters of each sample were trimmed respectively. The raw reads were mapped to the mouse (*Mus musculus*) genome (mm10) using STAR36 (2.4.2a) and annotated with transcriptome database (genecode vM13). Gene abundance estimation by reads count was conducted with the software RSEM37 (1.2.29). Normalized tags per million (TPM) were calculated on the number of clean reads mapped to specific region of genome using the relative log expression (RLE) method in edgeR38 (3.16.5). Differentially expressed genes (DEG) refer to compare gene expression level between two samples or two groups. DEG were defined by using the criterion that fold change >1.6 and adjust $p < 0.05$ (adjust p-value). We employed GSEA to explore the DEG and TPM. To perform GSEA, we utilized gene sets available on the Molecular Signatures Database website (Subramanian et al., 2005) (https://www.gsea-msigdb.org/) and a published data by Susan Chan' lab (Geimer Le Lay et al., 2014). Normalized Enrichment scores (NES) and false discovery rates (FDR) are denoted within the figures.

Real-Time PCR

Total RNA was extracted from the $CD8^+$ T cells with Trizol reagent. cDNAs were synthesized from 1 μg of total RNA using the SPARKscritpt II RT Plus Kit (SparkJade) and were amplified by 2×SYBR Green qPCR Mix (SparkJade) using Quantstudio 7 Real-Time PCR System (Life Technologies) according to the manufacturer's protocols. The information of primers for Real-Time PCR were provided in Table S1. Relative expression was calculated as $RQ = 2^{-\Delta\Delta Ct}$.

Mass spectral data

$CD8^+$ T cells were isolated and treated with DMSO, lenalidomide (10 μM) or pomalidomide (1 μM) for 24 h. After treatment, cell pellets were harvested by centrifugation at 400 × *g* for 5 min, washed in cold PBS, and flash frozen in liquid nitrogen. Cells were lysed in 8 M Urea, 50 mM NH_4HCO_3, supplemented with protease inhibitor cocktail, and sonicated with ultrasonic breaker (Scientz). Following lysis, samples were centrifuged at 15000 rpm for 12 min at 4°C. Proteins were quantified with the Pierce BCA Protein Assay Kit (Thermo Fisher). 100 μg proteins were reduced with 5 mM dithiothreitol for 1 h at room temperature (RT) and subsequently carbamidomethylated with 10 mM iodoacetamide for 30 min at RT in the dark. Samples were diluted to 1 M urea with 50 mM NH_4HCO_3, digested with sequencing grade trypsin (Promega) at an enzyme-to-substrate ratio of 1:50 at 37°C overnight with gentle rotation. Digested samples were acidified with 1% trifluoroacetic acid (TFA) (Sigma-Aldrich) and desalted on 50 mg tC18 Sep-Pak cartridges (Waters, WAT054960). Cartridges were conditioned with 1 mL 50%ACN/0.1% formic acid (FA), 1 mL 0.1% FA. Then samples were loaded onto a single cartridge, and subsequently washed twice with 1 mL of 0.1%FA. Samples were eluted from cartridges by washing twice with 1 mL of 50%ACN/0.1%FA. Desalted samples were dried in a Savant SC210A SpeedVac concentrator (Thermo Scientific).

Desalted peptides were separated and analyzed on an Easy-nLC 1200 system coupled to a Q Exactive HF-X (Thermo Scientific). Briefly, about 1 μg of peptides were separated in an Easy-Spray C18 column (75 μm × 50 cm, 2 μm, 100 Å, Thermo Scientific) at a flow rate of 250 nL/min at 50°C. Mobile phase A (0.1% formic acid in water) and mobile phase B (0.1% formic acid in 80% ACN) were used to establish a 90 min gradient. Peptides were then ionized by electrospray at 2.1 kV. A full MS spectrum (375–1500 *m/z* range) was acquired at a resolution of 120,000 at *m/z* 200 and a maximum ion accumulation time of 20 ms. Dynamic exclusion was set to 30 s. Resolution for HCD MS/MS spectra was set to 15,000 at *m/z* 200. The AGC setting of MS and MS^2 were set at 3E6 and 1E5 respectively. The 20 most intense ions above a 6.7E4 counts threshold were selected for fragmentation by HCD with a maximum ion accumulation time of 30 ms. Isolation width of 1.2 *m/z* units was used for MS^2. Single and unassigned charged ions were excluded from MS/MS. For HCD, normalized collision energy was set to 27%.

The raw data were processed and searched with MaxQuant 1.6.5.0 with MS tolerance of 4.5 ppm, and MS/MS tolerance of 20 ppm. The UniProt mouse protein database and database for proteomics contaminants from MaxQuant were used for database searches. Reversed database searches were used to evaluate false discovery rate (FDR) of peptide and protein identifications. Two missed cleavage sites of trypsin were allowed. Carbamidomethylation (C) was set as a fixed modification, and Oxidation (M), Acetyl (Protein N-term) and deamidation (NQ) were set as variable modifications. The FDR of both peptide identification and protein identification is set to be 1%. The option of ''Second peptides'' and ''Match between runs'' was enabled. Label-free quantification was used to quantify the difference of protein abundances between different samples.

Human specimens

The CRC specimens were obtained under a protocol approved by the institutional review board of Korea Advanced Institute of Science and Technology (4-2019-0811), and all patients provided written informed consent.

Tumor tissues were freshly dissociated for TIL isolation. $CD8^+$ T cells were magnetically enriched from peripheral blood mononuclear cells (PBMCs) and TILs using CD8 Micro-Beads (Miltenyi Biotec, 130-045-201) according to manufacturer's instructions. Non-$CD8^+$ cells were irradiated (3,000 rad) and used as feeder cells for stimulation. $CD8^+$ T cells were further sorted into $CD28^+$ and $CD28^-$subpopulations using FACS Aria II (BD Biosciences) with purity of >95%.

Sorted $CD28^+$ and $CD28^-$ $CD8^+$ T cells were labeled with CellTrace Violet (CTV; Invitrogen) in PBS with 5% fetal bovine serum for 20 min in 37°C incubator. To evaluate the effect of lenalidomide on activation and proliferation of $CD8^+$ T cells, CTV-labeled $CD28^+$ and $CD28^-$ $CD8^+$ T cells were stimulated with soluble anti-CD3 antibody (1 ng/mL; Miltenyi Biotec, 130-093-387) with or without lenalidomide (5 μM) in complete RPMI1640 media with irradiated autologous feeder cells. For combination treatment, anti-human PD-1 antibody (10 μg/mL; BioLegend, 329946) was added. After 108 h, cells were harvested, stained with viability dye for dead cell exclusion and antibodies against surface antigens, and analyzed by flow cytometry.

ELISA

The supernatant medium of $CD8^+$ T cells that were stimulated for 96 h was harvested for ELISA. IL2 and IFNγ were detected by ELISA kit (R&D) according to the manufacturer's protocols.

QUANTIFICATION AND STATISTICAL ANALYSIS

For all experiments, the number of technical and/or biological replicates (n) is provided in the figure legends or text. The number of mice in each treatment group was determined by power calculation, using the ''Sample size'' and ''stats19'' packages in R program, aimed for a power of 0.8 or greater. All statistical analyses were performed using GraphPad Prism 8 software. The definition of center, and dispersion and precision measures were clarified in the figure legends. Comparisons between two treatments were assessed using unpaired or paired (for matched comparisons) two-tailed Student's t-test, which were clarified in the figure legends. Grouped data were analyzed by multiple t-test, which were also clarified in the figure legends. In all cases, n.s. no significance *$p < 0.05$, **$p < 0.01$, ***$p < 0.001$, ****$p < 0.0001$.